Journal of Computational Applied Mechanics 2027, 58(1): 61-89

DOI: 10.22059/jcamech.2026.425442.1990

RESEARCH PAPER

Computational Fluid Dynamics Simulation of Non-Newtonian Pulsatile Blood Flow in Multi-Stenotic Arteries

O. Anwar Bég [a], M. N. Ali [b], Tasveer A. Bég [c], S. Kuharat [a], Ali Kadir [a], M.M. Bhatti [d,e,*], Henry J. Leonard [a]

[a] *Multi-Physical Engineering Sciences Group, Mechanical Engineering Department, Corrosion and Coatings Lab, Room 3-08, SEE Building, University of Salford, Manchester, M54WT, UK*

[b] *MSc Biomechanical Engineering Program, TU Delft, Mekelweg 2, 2628 CD Delft, Netherlands*

[c] *Engineering Mechanics Research, Israfil House, Dickenson Rd., Manchester, M13, UK*

[d] *Department of Physics, College of Science, Korea University, 145 Anam-ro, Seongbuk-gu, Seoul 02841, Republic of Korea*

[e] *Department of Mathematics and Natural Sciences, Center for Applied Mathematics and Bioinformatics (CAMB), Gulf University for Science and Technology, 32093 Hawally, Kuwait*

Abstract

Understanding the hemodynamic effects of arterial stenosis is critical for evaluating disease progression and treatment strategies. Motivated by deploying CFD visualization in this area, the present article conducts a numerical investigation of laminar blood flow in multi-stenosed arteries with varying degrees of stenosis: 50%, 70% and 90% area reduction, using ANSYS Fluent. Both Newtonian and non-Newtonian (Carreau) models were employed to analyse velocity, pressure, vorticity and wall shear stress (WSS) distributions. The Carreau model accounted for the shear-thinning behaviour of blood. The results demonstrated that increasing stenosis severity led to higher peak velocities within the constricted region, higher pressure drops, and a delayed flow recovery in severe cases. WSS was also found to increase significantly with stenosis severity, highlighting potential risk zones for plaque rupture. Furthermore, high vorticity and flow disturbances downstream of the stenosis indicated regions susceptible to recirculation and possibly thrombosis. These findings provide a foundation for future work that may involve generalization of curved complex arterial geometries, integration of Fluid-Structure Interaction (FSI) and potentially the use of turbulent flow models.

Keywords: Computational fluid dynamics (CFD); atherosclerosis; multiple stenoses; pulsatile blood flow; ANSYS FLUENT; non-Newtonian Carreau model; shear-thinning viscosity; wall shear stress (WSS).

1. Introduction

Arteries, veins and capillaries in the human body have a total length of approximately 60,000 miles, more than double the circumference of the entire Earth. The function of arteries is vital for maintaining good health. Yet, they are prone to diseases such as Atherosclerosis, which is defined as the hardening of arterial walls due to plaque

* Corresponding author. *E-mail address:* mmbhatti@korea.ac.kr

buildup. This plaque consists of fat, cholesterol or other substances. This buildup within the arterial walls leads to the narrowing of the arteries, a condition known as "stenosis", which can block blood flow and lead to various health problems such as heart attacks or strokes. Atherosclerosis is a very common cause which contributes to the development of cardiovascular disease (CVD). Research indicates that individuals over the age of 40, even those in good health, have a 50% likelihood of developing serious atherosclerosis [1]. The study of hemodynamics in stenotic arteries has been a critical area of research due to its direct implications for clinical diagnosis and treatments. A Particle Image Velocimetry (PIV) study by Geoghegan et al. [2] created a physically flexible carotid artery with an area stenosis of 75% and the flow behaviour was observed. As the high-speed flow exited the stenosis region, a reverse flow was recorded around it, forming vortices called Kelvin–Helmholtz instabilities. The flow was seen as axis-symmetrical, but with the increase in flow rate, those instabilities became asymmetrical, eventually leading to vortex breakdown.

Recent advancements in CFD modelling have focused on improving the accuracy of simulations through refined numerical methods and turbulence models. The study by Banks & Bressloff [3] investigated how turbulence influences blood flow in arteries with stenosis and bifurcations. They highlighted how stenosis leads to flow separation, recirculation zones and increased shear stress. Furthermore, the authors also compared different turbulence models to assess their accuracy and found the Shear Stress Transport (SST) k-ω model to be most effective in predicting complex arterial blood flow. This was further validated by Aghaee et al. [4] who compared various turbulence models in stenotic arteries and found that the transitional k-ω model provided the best balance between computational efficiency and accuracy in capturing turbulence effects. More recent studies used computational fluid dynamics (CFD) to predict stenosis effects on blood flow, such as the study by Kamangar et al. [5] where a patient-specific left coronary artery was modelled with area stenosis of 90% and 70%. It was concluded that the higher degree of stenosis induced a more severe influence including greater pressure drop, increased velocity and wall shear stresses. Akhtar et al. [6] modelled blood as laminar, incompressible and non-Newtonian Casson fluid model and showed the velocity increases as the flow enters the stenosis region and decreases, leaving the region. Similarly, Wu et al. [7] previously showed that flow velocity and wall shear stress (WSS) significantly rise with the severity of stenosis when the blood flow is modelled as pulsatile due to the effect of the cardiac cycle. Yang et al. [8] explored hemodynamic effects in varying segments of the carotid artery and found that stenosis location significantly alters blood velocity and pressure gradients.

While many early CFD studies modelled blood as a Newtonian fluid, recent research has emphasised the importance of non-Newtonian properties in accurately simulating blood flow. For example, Liu et al. [9] analysed blood flow in a 75% stenosis using Casson and Carreau-Yasuda non-Newtonian models and concluded that the non-Newtonian model predicts higher wall shear stress (WSS) near the stenosis compared to the Newtonian model. Singh and Shah [10] compared Newtonian and non-Newtonian models in stenotic arteries and concluded that non-Newtonian behaviour significantly impacts WSS and flow separation, particularly in severe stenosis conditions. Erwin and Marpaung [11] examined both Newtonian and non-Newtonian models and revealed that the Newtonian model fails to accurately represent the complexities of blood behaviour in stenosed regions. Furthermore, the Carreau-Yasuda model was identified to be the most suitable when modelling fluid viscosity in constricted artery sections. The theoretical study by Dubey et al. [12] and others simulated the complex blood properties by introducing a two-fluid non-Newtonian model where the Casson model was applied to the core region of blood flow and the Sisko model for the peripheral porous region of the artery to better capture the shear-thinning effects of blood. It was noted that the stenosis increases velocity and wall shear stress (WSS), which can lead to endothelial damage and aneurysms, slow blood flow and reduce shear stress, potentially leading to clot formation. Zhou et al. [13] showed using the Carreau-Yasuda model that blood flow separation and vortex formation occur immediately after the stenotic region in diseased arteries. Likewise, another study by Yaghoub et al. [14] used the same Carreau-Yasuda model when modelling small arteries. The findings discovered a considerable pressure drop with an area stenosis of more than 60%. This phenomenon is further validated by Rahma et al. [15], where the authors performed a CFD simulation on a patient-specific cerebral artery through MRI scans and found the pressure drop significantly increases during the contraction when the area ratio is increased.

These investigations highlight that Computational Fluid Dynamics has transformed the study of blood flow in stenotic arteries, providing critical insights into turbulence, pressure drops, and other characteristics. These advancements have improved the precision of simulations while also contributing to a deeper understanding of the relationship between arterial narrowing and blood flow patterns. Consequently, CFD has become an essential tool for the analysis of cardiovascular care.

Most previous studies of hemo-rheological blood flows have considered single stenosis and ignored multiple stenoses effects [16, 17]. The present article therefore conducts a numerical investigation of laminar blood flow in multi-stenosed arteries with varying degrees of stenosis: 50%, 70% and 90% area reduction. ANSYS Fluent software [18, 19] is deployed. Both Newtonian and non-Newtonian (Carreau) models are utilized to analyse velocity,

pressure, vorticity and wall shear stress (WSS) distributions. Although we consider only 2-D simulations, a solid platform is established for future extensions to 3-D simulations.

2. Modelling and blood flow physics

The fluid considered for this study is blood. Blood is considered a non-Newtonian fluid because its viscosity is not constant but changes with the shear rate. However, under specific conditions, blood may be denoted as a Newtonian fluid. This complex behaviour occurs because the fluid contains plasma (a Newtonian fluid) and other cellular components like red blood cells, white blood cells, and platelets. In large arteries such as the Aorta, during fast blood flow, the shear rate increases and becomes relatively high (>100 s-1). In return, the viscosity reduces and becomes nearly constant. Hence, the blood behaves like a Newtonian fluid. On the contrary, in small capillaries, the flow velocity is lower; here, the red blood cells aggregate to form rouleaux structures as noted in Weisel & Litvinov [20]; this significantly increases viscosity, and the blood behaves like a non-Newtonian fluid. Since blood mostly exhibits non-Newtonian behaviour, a non-Newtonian mathematical model is used to represent this type of behaviour. Inspection of the literature has revealed that while various non-Newtonian models have been used previously, the Carreau model remains very popular as noted by Yaghoub et al. [14] and Erwin & Marpaung [11], in CFD simulations for its accuracy when capturing the blood flow behaviour in small arteries. Hence, this is the chosen mathematical model for this study, and this model is available in the "materials physics" options in ANSYS Fluent software.

2.1. Navier Stokes Equations

Laminar, viscous blood flow is assumed. For large vessels (like arteries), blood can often be approximated as a Newtonian fluid because shear rates are high, and viscosity remains almost constant. The Navier-Stokes equations represent the mathematical foundation for Newtonian fluid flow modelling, particularly under the assumption of a constant dynamic viscosity (μ) independent of the shear rate. The governing conservation equations in an (*x,y*) coordinate system for the general 2-D unsteady hemodynamic case, are:

Mass conservation:

$$\left[\frac{\partial u}{\partial x}+\frac{\partial v}{\partial y}\right]=0 \tag{1}$$

x-direction momentum conservation:

$$\rho\left[\frac{\partial u}{\partial t}+u\frac{\partial u}{\partial x}+v\frac{\partial u}{\partial y}\right]=\rho F_x-\frac{\partial p}{\partial x}+\mu\left[\frac{\partial^2 u}{\partial x^2}+\frac{\partial^2 u}{\partial y^2}\right] \tag{2}$$

y-direction momentum conservation:

$$\rho\left[\frac{\partial v}{\partial t}+u\frac{\partial v}{\partial x}+v\frac{\partial v}{\partial y}\right]=\rho F_y-\frac{\partial p}{\partial y}+\mu\left[\frac{\partial^2 v}{\partial x^2}+\frac{\partial^2 v}{\partial y^2}\right] \tag{3}$$

Here (*u, v*) are the (*x, y*) co-ordinates, P is pressure (Pa), ρ is fluid density (kg/m^3), μ is dynamic viscosity (kg/ms), $v=\mu/\rho$ is kinematic viscosity (m^2/s), t the time, F_x, F_y, are the body forces (which may be gravitational, body acceleration etc.) (N), $\frac{\partial p}{\partial x}$ is the *x*-direction pressure gradient and $\frac{\partial p}{\partial y}$ is the y-direction pressure gradient. Blood can be modelled as Newtonian (for larger vessels) but is non-Newtonian in narrower vessels e.g. stenotic geometries, so the Navier-Stokes equations must be modified with a rheological model. e.g. Carreau shear-thinning, which is available in ANSYS FLUENT CFD software [20].

2.2. Carreau Fluid model

Named after a renowned rheologist Pierre Carreau, the Carreau fluid model is a mathematical representation used in fluid mechanics and biomechanics to characterise non-Newtonian behaviour of fluids where the viscosity changes with shear rate. The model is particularly effective for describing shear-thinning fluids such as blood or polymer solutions. The relationship between shear viscosity (μ) and shear rate ($\dot{\gamma}$) can be expressed through this model:

$$\mu(\dot{\gamma})=\mu_\infty+(\mu_0-\mu_\infty)[1+(\lambda\dot{\gamma})^2]^{\frac{n-1}{2}} \tag{4}$$

Here μ_0: Zero-shear viscosity (Pa.s) [viscosity at very low shear rates], μ_∞: Infinite-shear viscosity (Pa.s), [viscosity at very high shear rates], λ: Characteristic time (s), [relates to the fluid's relaxation time], *n*: rheological power-law index, $\dot{\gamma}$: Shear rate (s^{-1}) and rheological power-law index *n* describes the degree of shear-thinning. Three cases are of interest i.e. $n = 1$: Newtonian fluid, $n < 1$: Shear-thinning fluid (pseudoplastic) and $n > 1$: Shear-

thickening fluid (dilatant). In order to use this model for this study, the constants in Eq. (4) need to be known to represent blood. The values were extracted from Cho & Kensey et al. [21].

Table 1: **Carreau model constants for blood**

Time constant λ (s)	**3.313**
Power-law index n	0.3568
Zero shear viscosity $\mu_0(kg/ms)$	0.056
Infinite shear viscosity μ_∞(kg/ms)	0.0035
Shear rate $\dot{\gamma}$ (s^{-1})	200

The Carreau model is particularly useful in near-plaque, low-shear zones, where viscosity rises and WSS decreases, conditions strongly associated with platelet activation and thrombosis. Selection of the Carreau model option in ANSYS FLUENT modifies the appropriate terms in the basic Newtonian viscous model. Many successful applications of this model have been communicated in previous studies of biomedical flows including stenotic hemodynamics [22], peristaltic blood micro-pumps [23], biosensors [24], biomaterials processing [25] and bifurcated blood flows [26]. A key hemodynamic parameter is the wall shear stress (WSS) which is useful for predicting and estimating distributed flow conditions and the development of local atherosclerotic plaque. It is computed using:

$$\tau_w = \mu \frac{\partial u}{\partial y} = \mu \cdot \dot{\gamma} \tag{5}$$

Here $\dot{\gamma}$ is deformation rate and $\frac{\partial u}{\partial y}$ is axial spatial velocity gradient.

3. Ansys fluent CFD modelling

This study adopts a computational fluid dynamics CFD approach to investigate laminar, unsteady, incompressible blood flow in a two-dimensional multi-stenosed artery. The methodology is designed to capture the hemodynamic characteristics of blood under pulsatile flow conditions, incorporating its shear-thinning behaviour through a non-Newtonian viscosity (Carreau model). We describe each stage of the CFD simulations below:

3.1. Geometry Creation - Design of the Multi-Stenotic Artery Models

To examine the effects of arterial stenosis on blood flow, three 2D arterial models were developed with varying degrees of area stenosis: 50%, 70%, and 90%. Since the analysis of velocity, pressure, and shear stress is typically performed on a 2D plane, even in 3D simulations, simplifying the model to 2D significantly reduces computational cost while still capturing the essential hemodynamic characteristics. The artery was modelled with a diameter of 5 mm, which is representative of small arteries such as the coronary arteries or common carotid artery branches, where diameters typically range from 3 mm to 9 mm (Goubergrits et al. [27]). The model was divided into three key regions: pre-stenosis, stenosis, and post-stenosis. The pre-stenotic segment was assigned a length of 20 mm to ensure that blood flow could fully develop before reaching the stenosis. A similar 20 mm length was used for the post-stenotic region, allowing sufficient space for disturbed flow to recover and providing an adequate region for analysing flow separation and vortex formation. The stenosis itself was designed with a length of 10 mm, which is twice the diameter of the artery. This choice is supported by previous research, notably Beatt et al. [28], which found that a stenosis length of approximately two times the vessel diameter effectively captures the flow disturbances associated with arterial narrowing while maintaining a computationally manageable model. The dimensions for all components of the geometric stenotic blood vessel model are summarized in Table 2. Figs. 1-3 visualize the three dual stenotic depth cases (50%, 70%, and 90%) to be simulated. All models are created in ANSYS workbench sketch tool.

Table 2: Dimensions adopted for the dual stenotic arterial models

Parameter	Dimension
Artery Diameter	5 mm
Pre-Stenosis Length	20 mm
Stenosis Length	10 mm
Post-Stenosis Length	20 mm
Total Length	80 mm
Area Stenosis Severity	50%, 70%, 90%

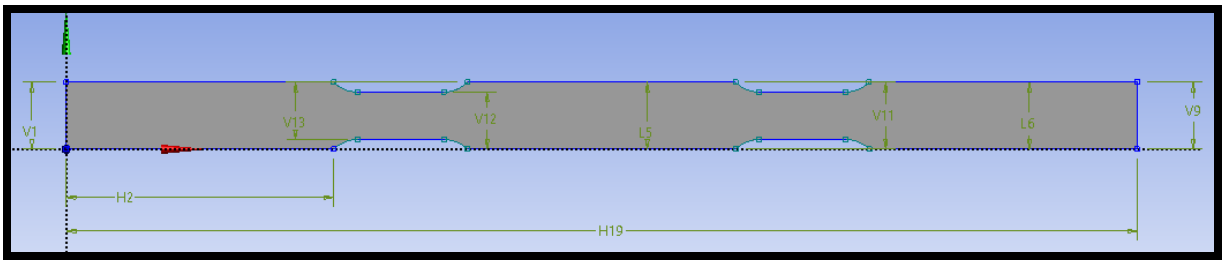


Figure 1: 50% Area Dual Stenosis Geometry

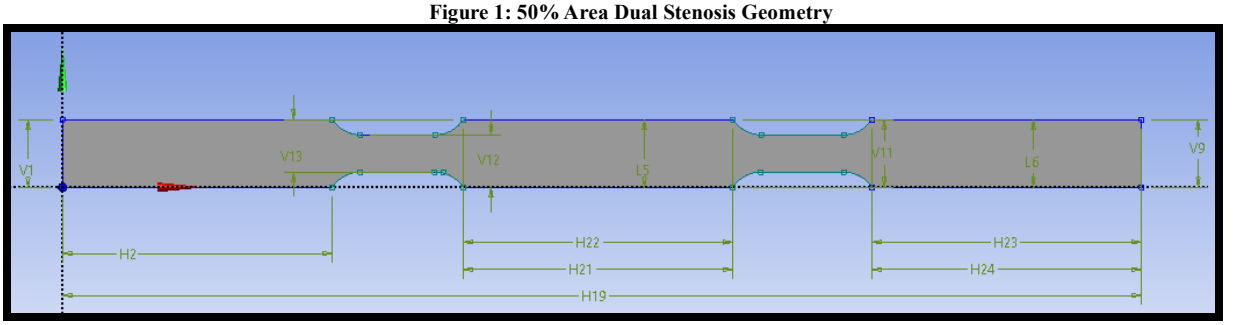


Figure 2: 70% Area Dual Stenosis Geometry

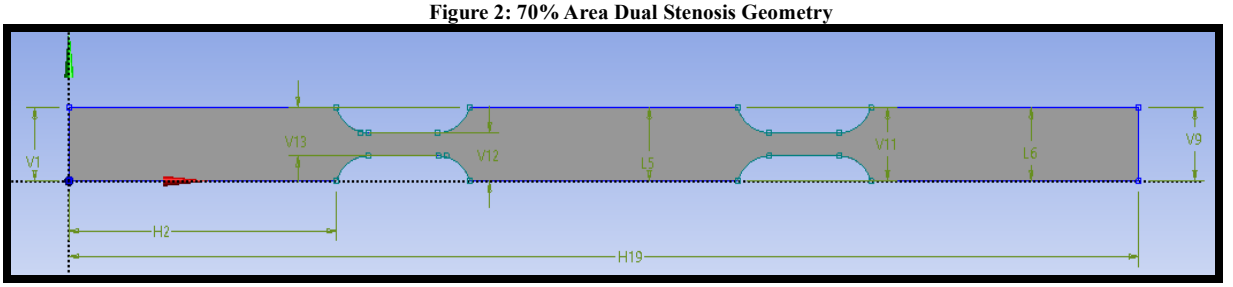


Figure 3: 90% Area Dual Stenosis Geometry

3.2. Pulsatile Flow

As mentioned above, the flow considered throughout this study was unsteady i.e. transient, which means the inlet velocity varies depending on time. This is due to the pulsatile nature of real blood flow which is associated with the systolic/diastolic stages of the cardiac cycle and heart pumping. This was simulated by using a User-Defined Function (UDF) within ANSYS Fluent. A UDF is a .c type file which is uploaded to Fluent and is interpreted by the software. This was used while setting the boundary conditions at the inlet. The velocity ranges from 0.1 m/s to 0.5 m/s as defined in the function. This was verified later to ensure the function was working as expected, as can be seen in Figure 4.

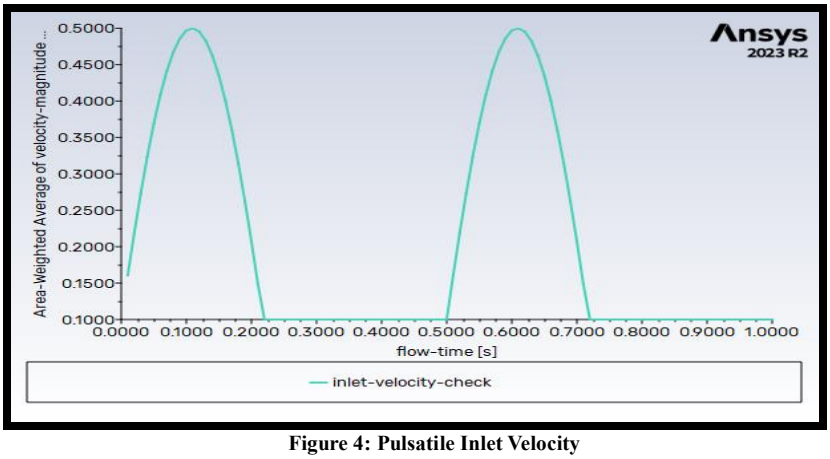


Figure 4: Pulsatile Inlet Velocity

3.3. Area Stenosis (AS) Calculations

The area stenosis % (S) is given by:

$$S = \left(1 - \frac{A_{stenosis}}{A_{original}}\right) \times 100 \tag{6}$$

Here $A_{original} = \frac{\pi D^2}{4} (original\ cross - sectional\ area\ of\ blood\ vessel)$,

$A_{stenosis} = \frac{\pi d^2}{4} (reduced\ i.e.\ stenotic\ cross - sectional\ area)$,

$D = original\ diameter\ (5\ mm)$,

$d = stenosis\ diameter$ (mm).

Rearranging for *stenosis diameter*, d gives:

$$d = D\sqrt{1 - S} \tag{7}$$

Calculating d for each stenosis severity case:

1. 50% AS: $d = 5\sqrt{1 - 0.50} = 3.54\ mm$
2. 70% AS: $d = 5\sqrt{1 - 0.70} = 2.74\ mm$
3. 90% AS: $d = 5\sqrt{1 - 0.90} = 1.58\ mm.$

3.4. Mesh Design and Convergence Study

The 2-D multi-stenotic geometry is meshed with quadrilateral elements. For accurate results, 10 inflation layers are added to the wall. The mesh generated is shown in Fig. 5.

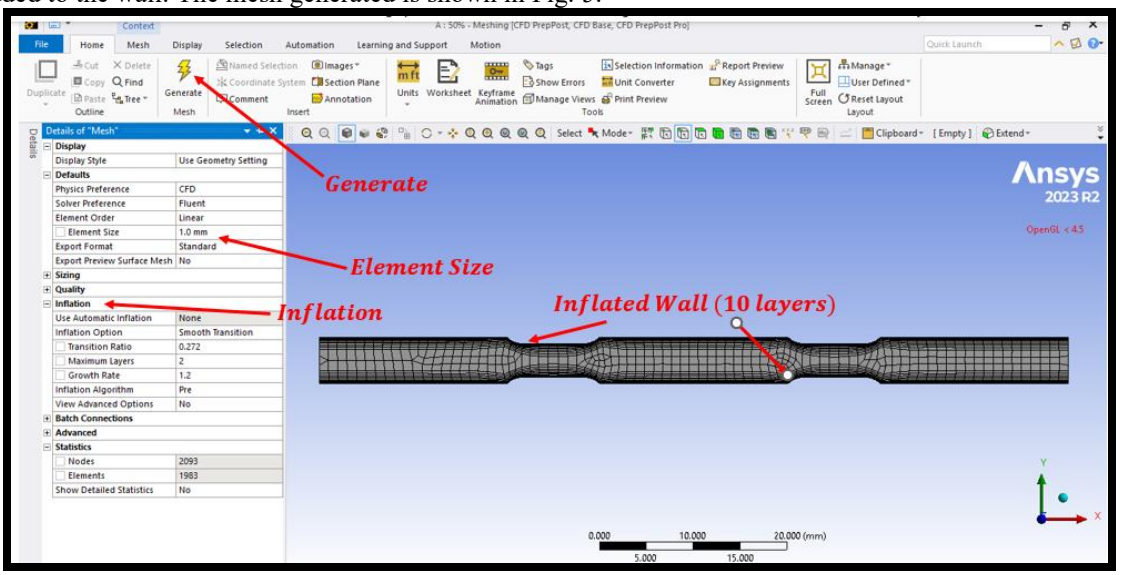


Figure 5: Mesh design for dual stenotic arterial model

The initial element size was selected as 2.0 mm, which was reduced when the mesh was refined.

A uniform element size of 0.5 mm was eventually deployed for mesh generation across all geometries, as determined through a mesh refinement study (Table 3 and Fig. 6). The mesh consisted of a combination of quadrilateral and tetrahedral elements. The total number of elements varied slightly between models, with the 50% area stenosis (AS) geometry containing 8,980 elements, the 70% AS geometry having 8,721 elements, and the 90% AS geometry with 8,650 elements.

Table 3: Element size against maximum velocity value

Element Size (mm)	Number of Elements	Maximum Velocity Magnitude (m/s)
2	1419	0.1896705
1	1983	0.1892031
0.5	4307	0.1976681
0.4	5889	0.1977004
0.3	8980	0.1979884

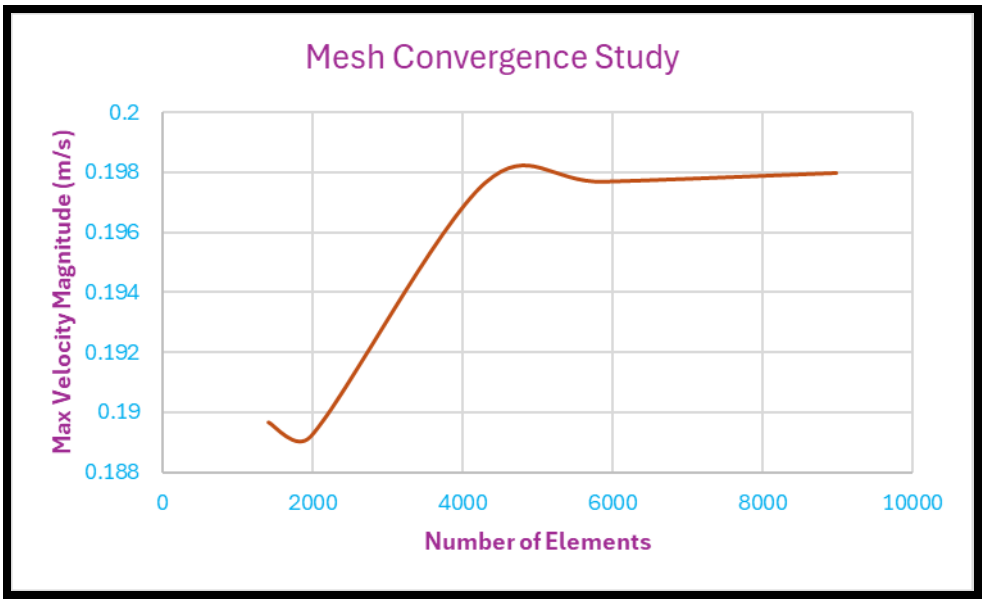


Figure 6: Mesh convergence study

The effect of mesh refinement was examined on the maximum velocity magnitude. As shown in **Figure 6**, the velocity initially fluctuated but gradually stabilised beyond approximately 6000 elements, indicating mesh independence. The chosen element size was 0.5 mm, which provided a balance between computational efficiency and result accuracy. The percentage error between the 0.5 mm mesh and an extremely refined 0.3 mm mesh was calculated to be 0.16%, confirming that further refinement had a negligible impact on the results. This indicates that the 0.5 mm mesh is sufficiently fine to capture accurate results without excessive computational cost.

3.5. ANSYS FLUENT Solver

The pressure-based SIMPLE solver in ANSYS FLUENT is utilised [18, 19] and this employs the finite volume method (FVM) to solve the governing equations either sequentially using a segregated algorithm or simultaneously through a coupled algorithm. Blood was assumed to be laminar, incompressible, and transient throughout the simulations. The assumption of laminar flow is reasonable for small arteries, such as the coronary arteries, where Reynolds numbers typically remain below the threshold for turbulence under normal physiological conditions as noted in Ku [16]. Additionally, a transient flow model was selected to accurately represent the pulsatile nature of blood flow, ensuring that velocity and pressure fluctuations are realistically captured.

3.6. Boundary conditions

As noted earlier, we deploy a User-Defined Function (UDF) for the pulsatile flow for which the inlet velocity will vary between 0.1 m/s to 0.5 m/s. Human blood pressure is measured using two values: Systolic pressure and Diastolic Pressure.

Systolic blood pressure – the pressure exerted on artery walls when the heart contracts and pumps blood, representing the highest pressure in the arteries. 120 mmHg in healthy adults.

Diastolic blood pressure – the pressure in the arteries when the heart is at rest between beats, indicating the lowest pressure in the circulatory system. 80 mmHg in healthy adults.

To accommodate for this, the outlet pressure was also changed while applying the boundary conditions. 100 mmHg was used (13332 Pa).

Once all the boundary conditions are applied, the solution needs to be calculated, prior to which ANSYS FLUENT requires initial values for flow variables (e.g. velocity, pressure, etc). to determine those values. We deploy hybrid initialization with the number of iterations set to initially 1000 and a reporting interval of 1. Figure 7 shows the residuals where the solution converges after 32 iterations; this happened for the constant inlet velocity case, which was used for the mesh convergence study, as a constant velocity takes much less computation power to solve. After the UDF was added, the solution converged after 1200 iterations.

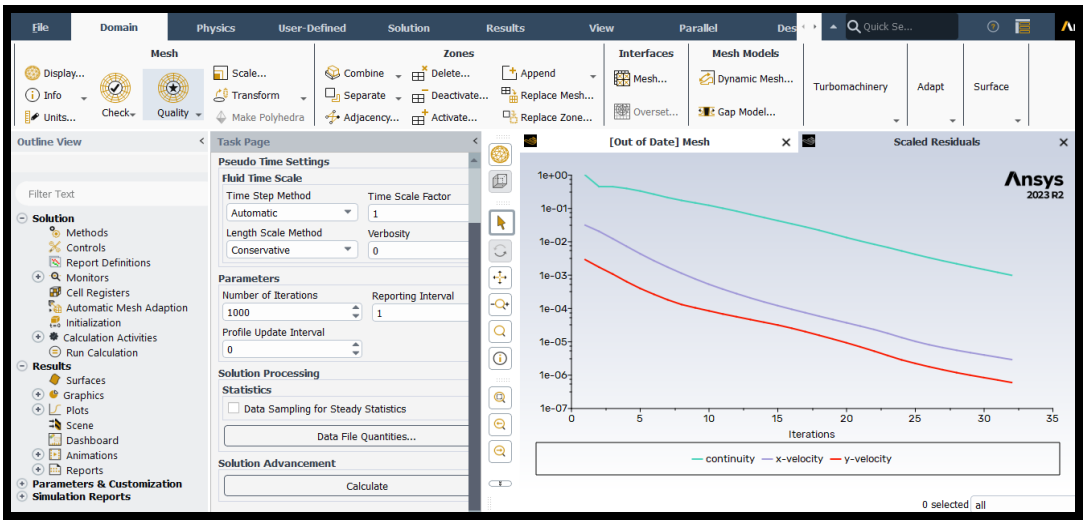


Figure 7: **Running the CFD simulation and residual iterations**

3.7. Postprocessing

Good practice in CFD simulation is to verify the solution first before analysing the results. One way to do this is to check mass conservation. The net result of the mass flow rate at the inlet and outlet should be zero or very close to zero.

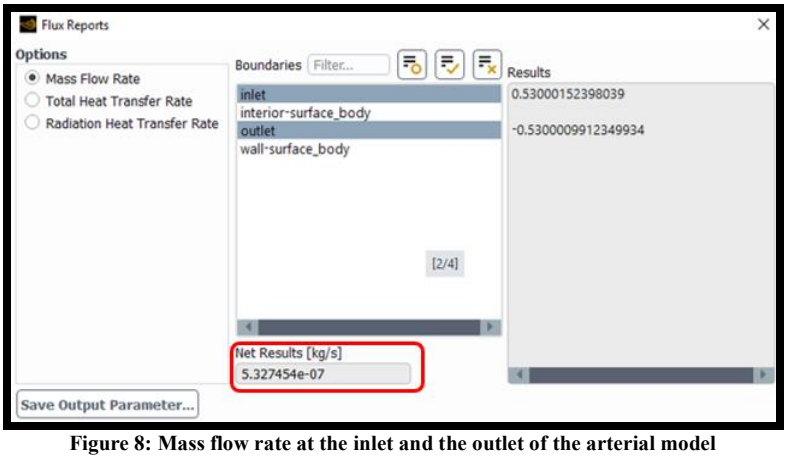


Figure 8: Mass flow rate at the inlet and the outlet of the arterial model

Fig. 8 shows a mass flow rate of 5.32×10^{-7}, which is acceptable as it is extremely small. This verifies the ANSYS FLUENT solution. Different contour plots can then be extracted at this stage (e.g. *velocity, pressure, wall shear stress, vorticity* etc) and all simulation results are described in the next section.

4. ANSYS FLUENT results and discussion

Contour plots were used to visualise key flow characteristics within the stenosed artery. *Velocity, pressure, and vorticity* contours were selected for both Newtonian and non-Newtonian fluids to provide a comprehensive understanding of hemodynamic behaviour. For wall shear stress (WSS), the maximum values were collected for both fluids and plotted on a bar chart to compare and visualise the differences in WSS values between various stenosis depths. All visualizations are shown in the following subsections.

4.1. Velocity Contours

Figures 9-26 display the contours of velocity. We consider intermediate (50%) i.e. Figs 9-14, strong (70%) i.e. Figs. 15-20 and chronic stenosis (90%) i.e. Figs 21-26, in turn. Each stenosis severity case has 6 plots- *Newtonian, non-Newtonian, Newtonian Systolic, Newtonian Diastolic, non-Newtonian Systolic and non-Newtonian Diastolic.* A consistent trend can be seen regardless of the stenosis depth, where the maximum velocity occurs in the constricted

region, as the area decreases and the blood has less space to transport through, indicated by the red colour in the contours.

4.1.1. 50% Area Stenosis (AS)

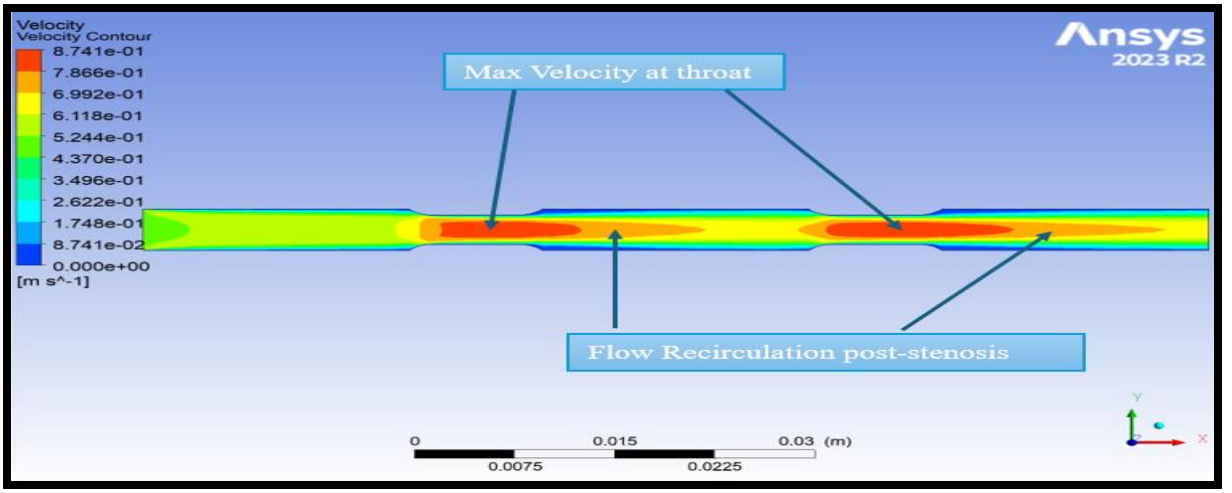


Figure 9: Velocity Magnitude at 50% AS: Newtonian Model

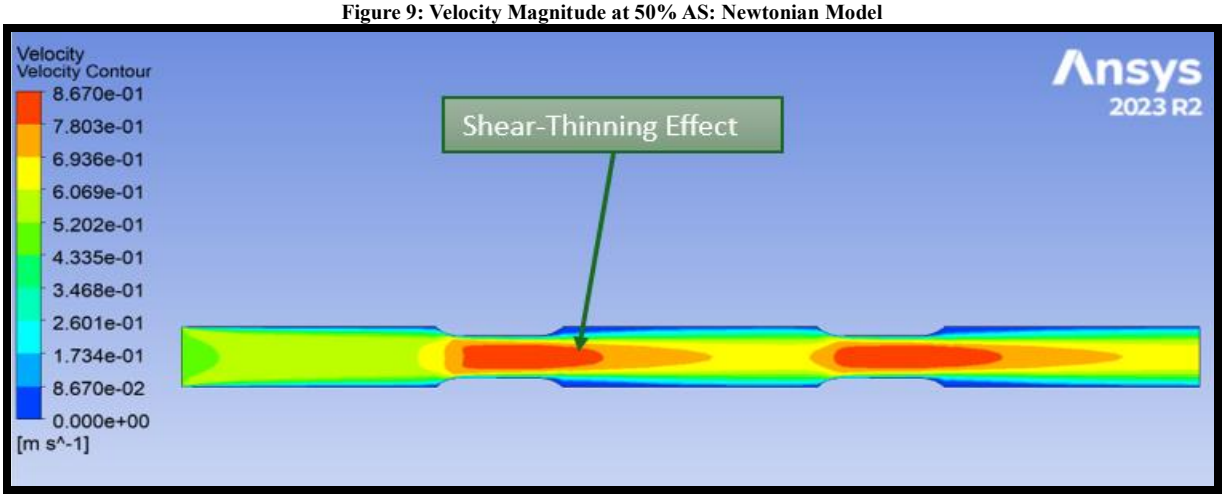


Figure 10: Velocity Magnitude at 50% AS: non-Newtonian Carreau Model

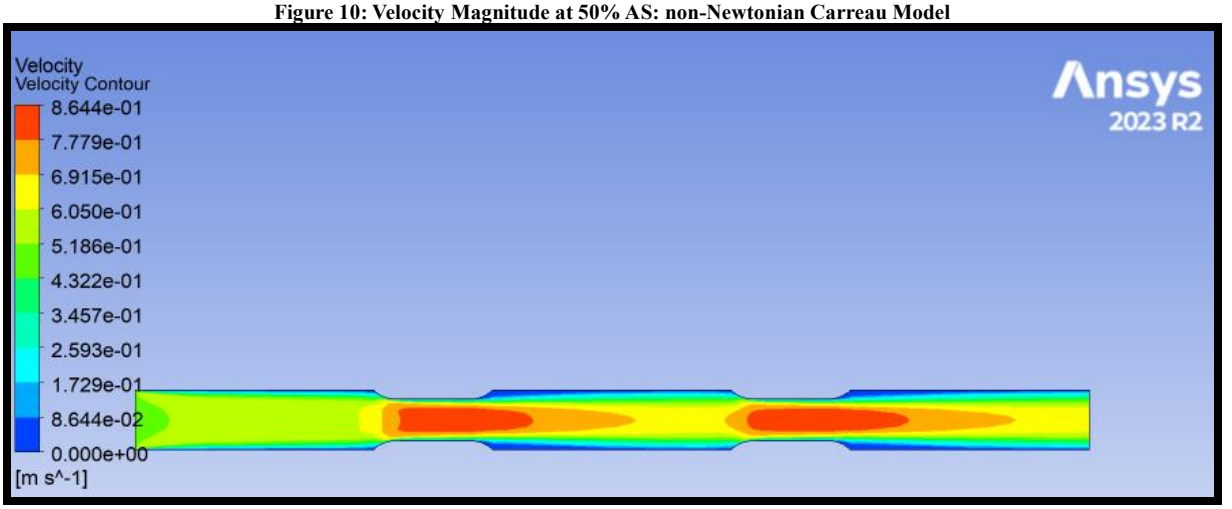


Figure 11: Velocity Magnitude at 50% AS: Newtonian Systolic

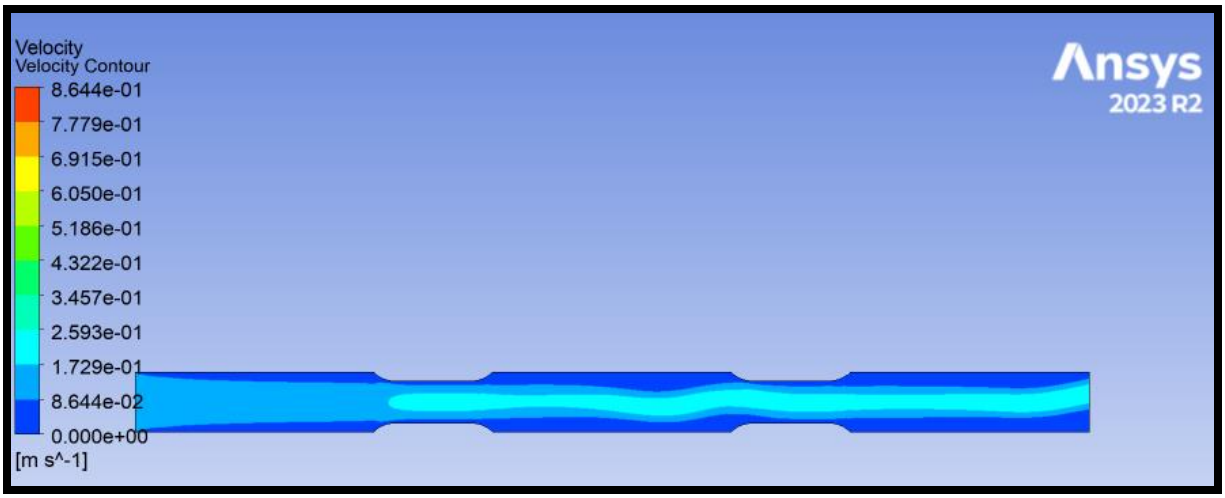


Figure 12: Velocity Magnitude at 50% AS: Newtonian Diastolic

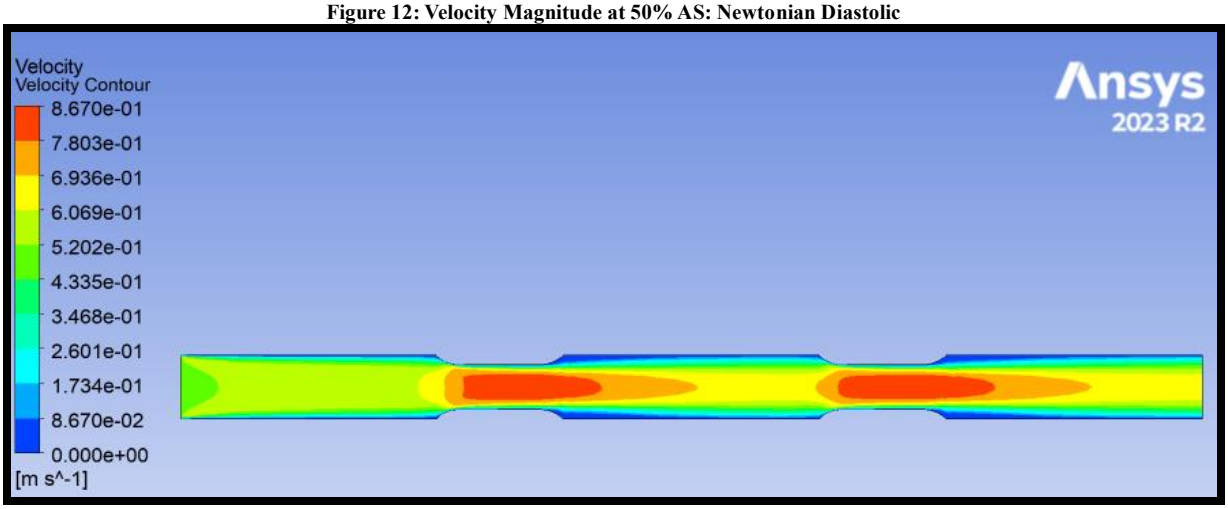


Figure 13: Velocity Magnitude at 50% AS: non-Newtonian Carreau Systolic

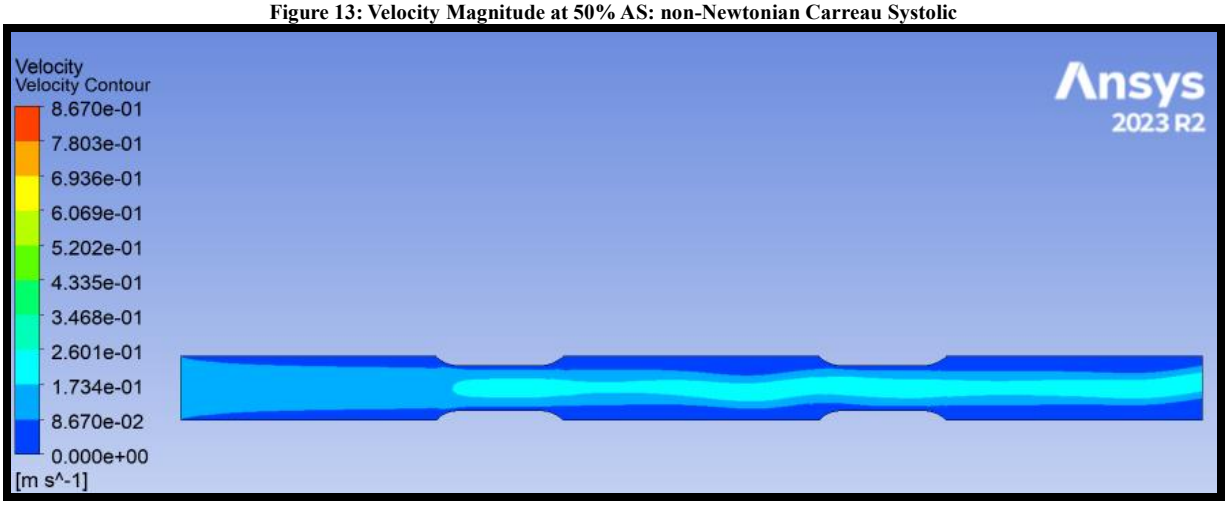


Figure 14: Velocity Magnitude at 50% AS: non-Newtonian Carreau Diastolic

4.1.2. 70% Area Stenosis (AS)

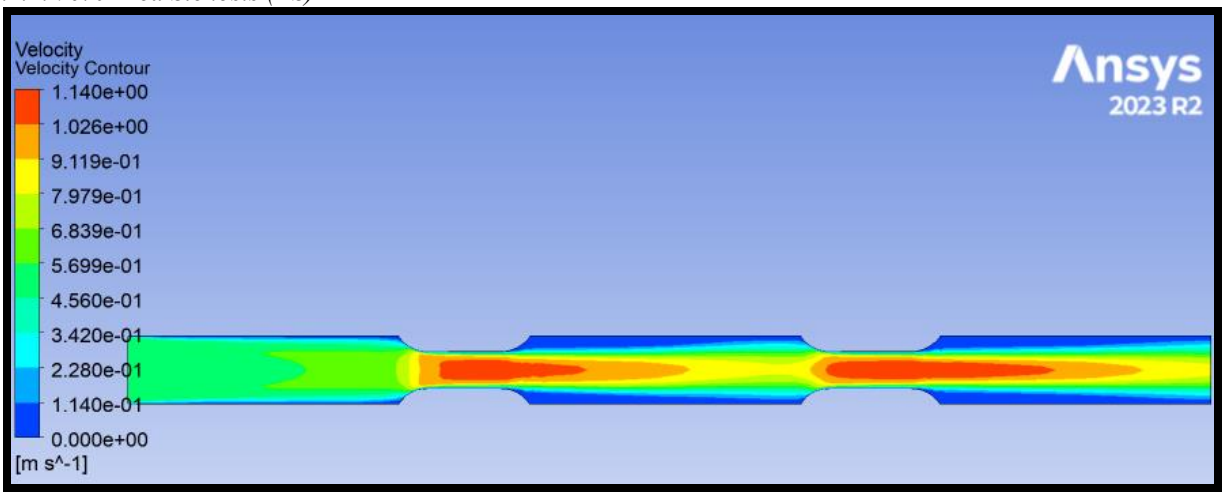


Figure 15: Velocity Magnitude at 70% AS: Newtonian Model

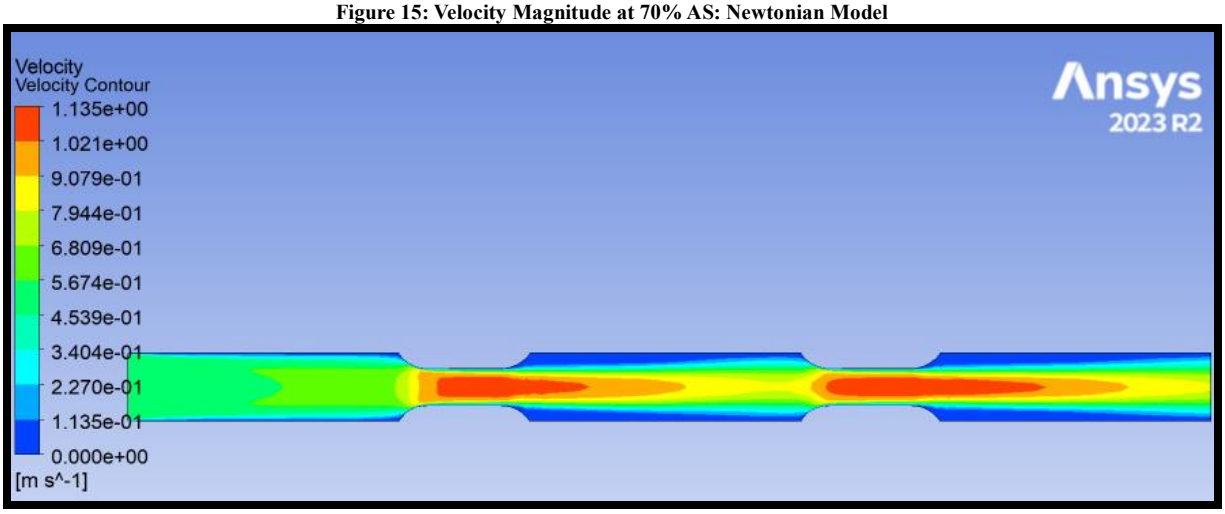


Figure 16: Velocity Magnitude at 70% AS: non-Newtonian Carreau Model

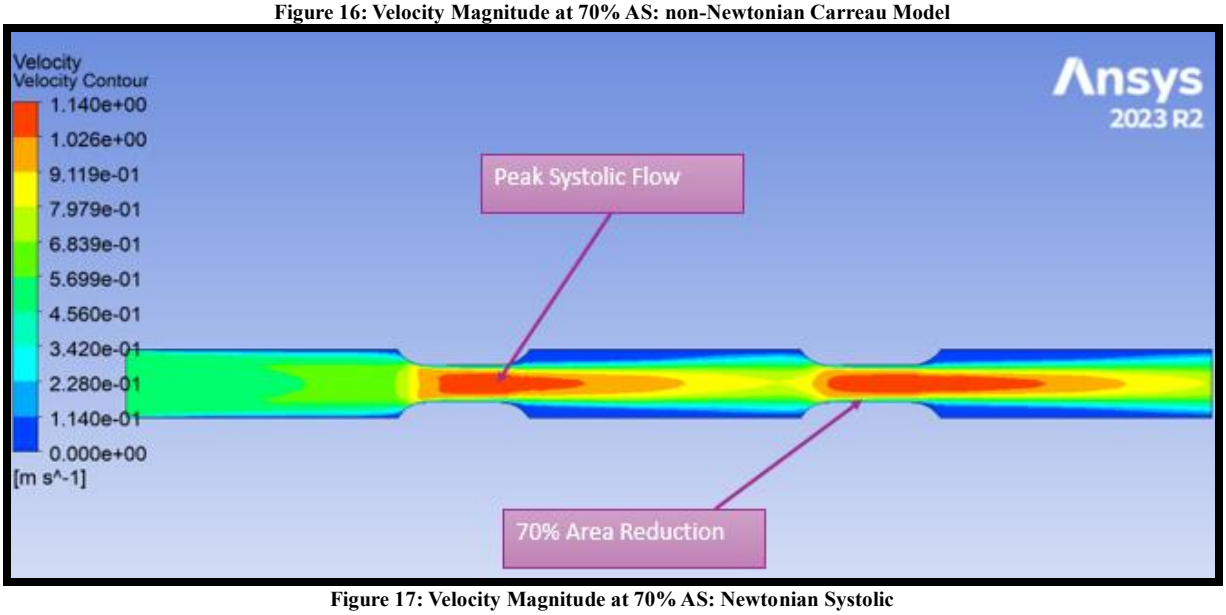


Figure 17: Velocity Magnitude at 70% AS: Newtonian Systolic

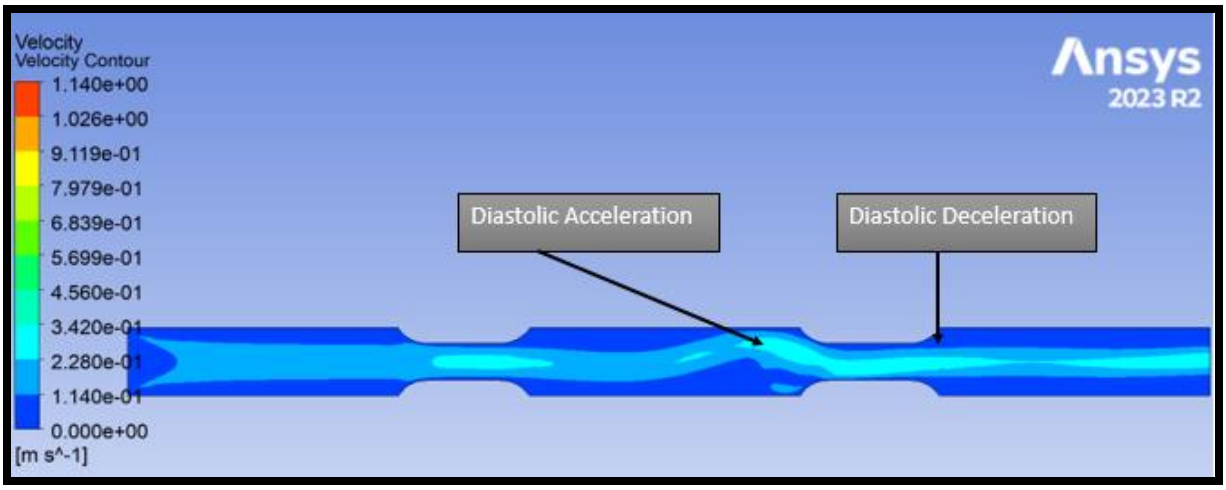


Figure 18: Velocity Magnitude at 70% AS: Newtonian Diastolic

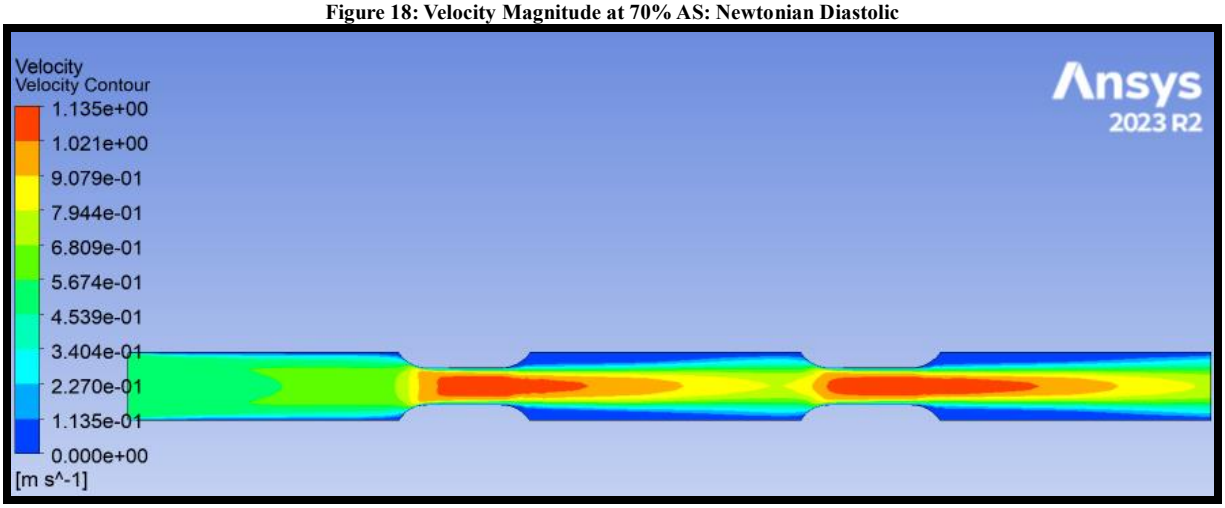


Figure 19: Velocity Magnitude at 70% AS: non-Newtonian Carreau Systolic

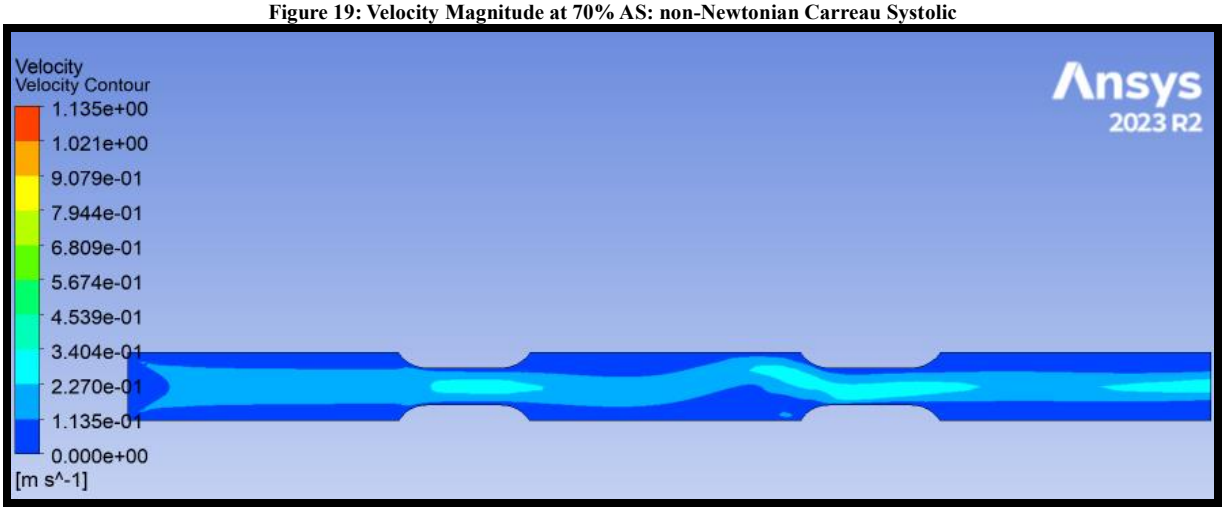


Figure 20: Velocity Magnitude at 70% AS: non-Newtonian Carreau Diastolic

4.1.3. 90% Area Stenosis (AS)

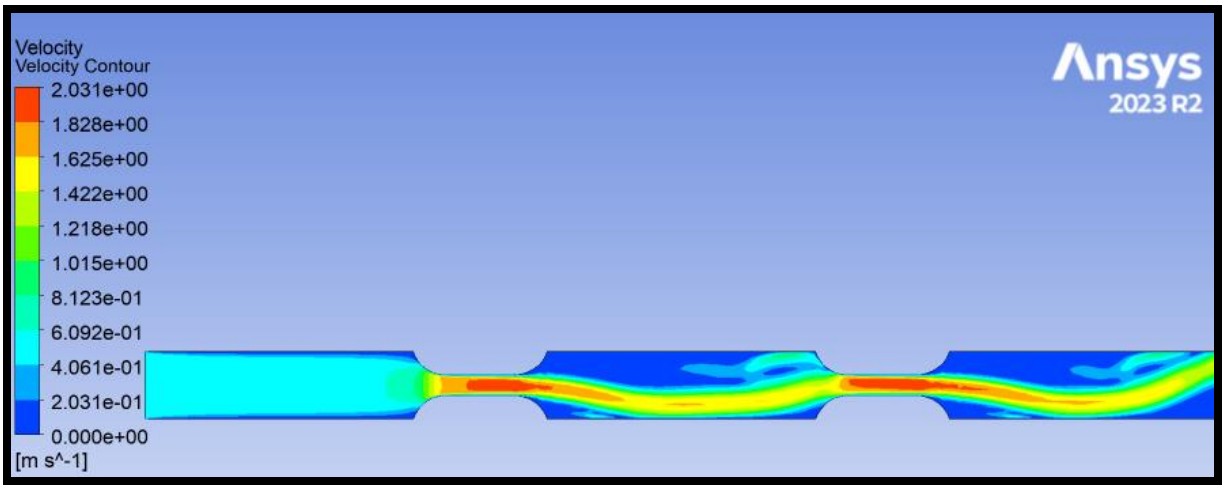


Figure 21: Velocity Magnitude at 90% AS: Newtonian Model

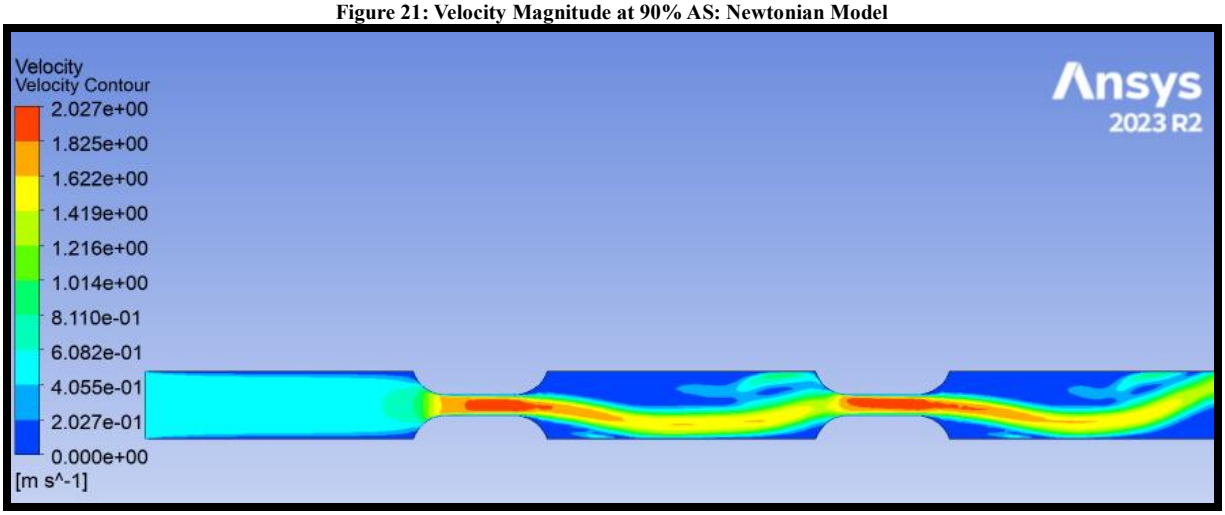


Figure 22: Velocity Magnitude at 90% AS: non-Newtonian Carreau Model

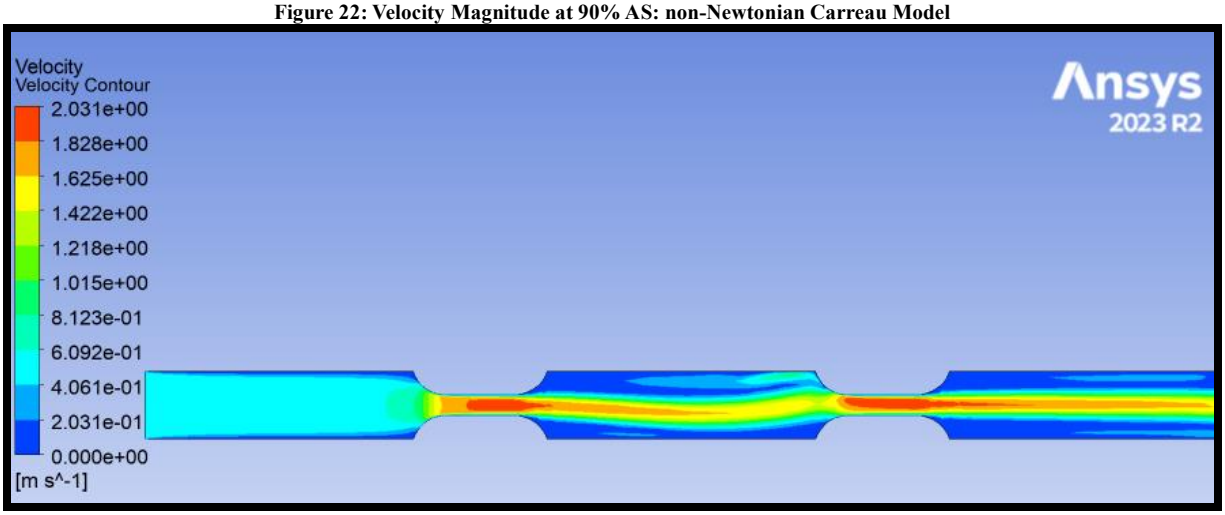


Figure 23: Velocity Magnitude at 90% AS: Newtonian Systolic

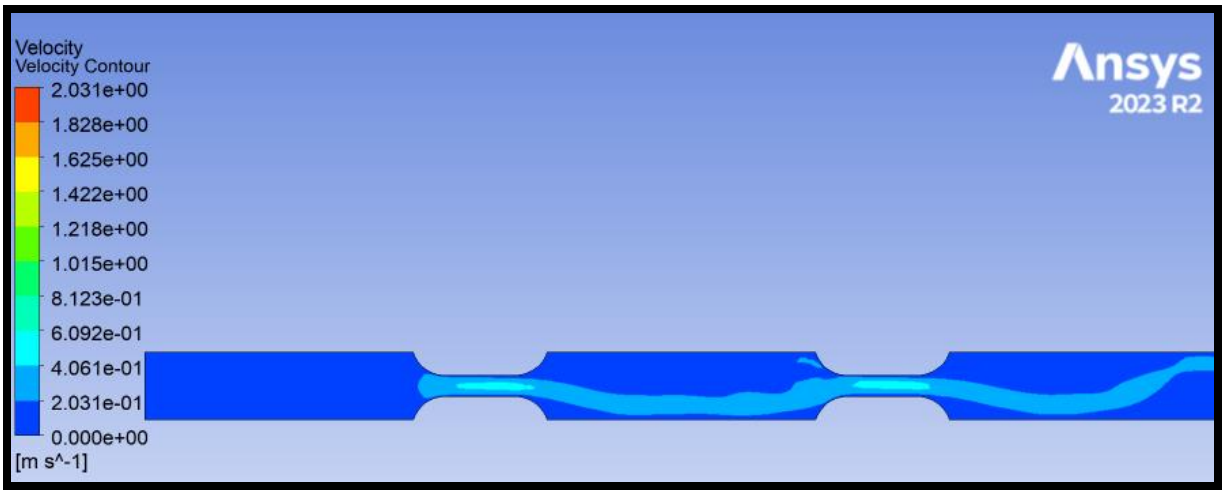


Figure 24: Velocity Magnitude at 90% AS: Newtonian Diastolic

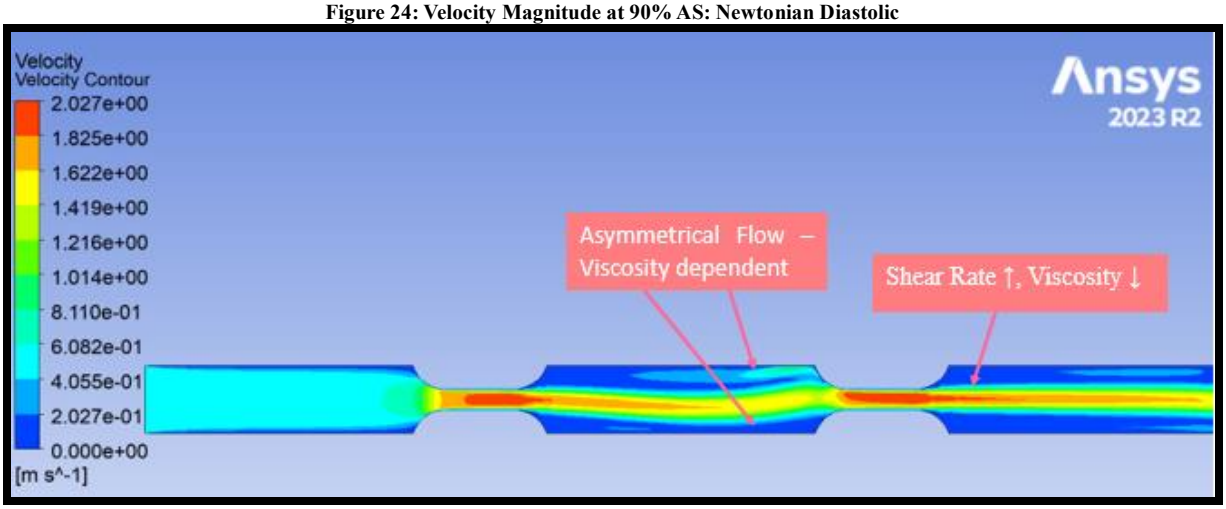


Figure 25: Velocity Magnitude at 90% AS: non-Newtonian Carreau Systolic

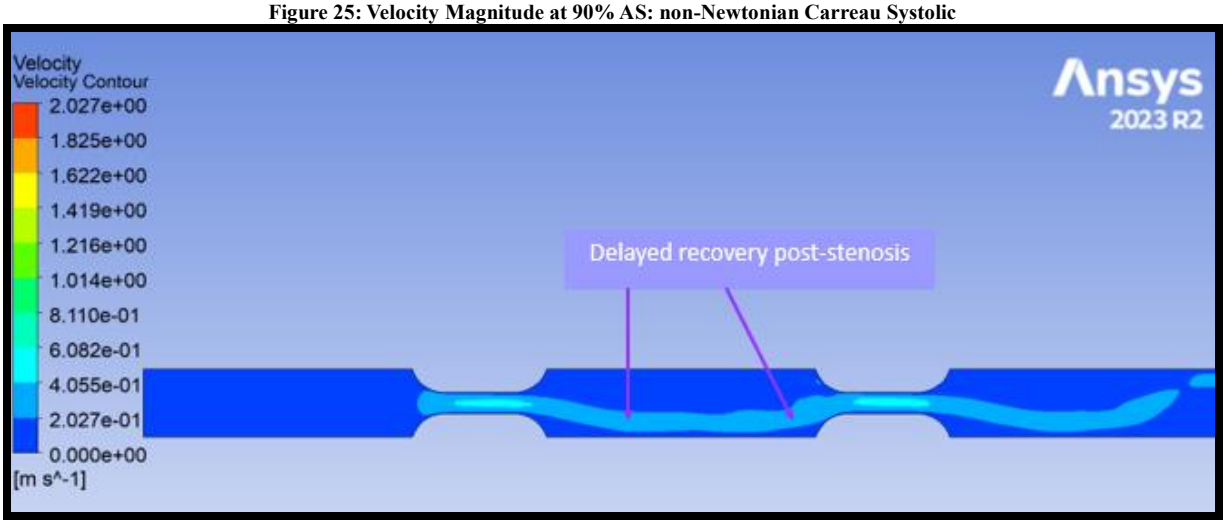


Figure 26: Velocity Magnitude at 90% AS: non-Newtonian Carreau Diastolic

At the stenosis, the arterial lumen is most constricted, causing a significant acceleration of flow. In the cases of 50% and 70% stenosis, the velocity reaches its peak before slowly declining downstream, forming a jet-like structure, which is zoomed in Figure 27 below.

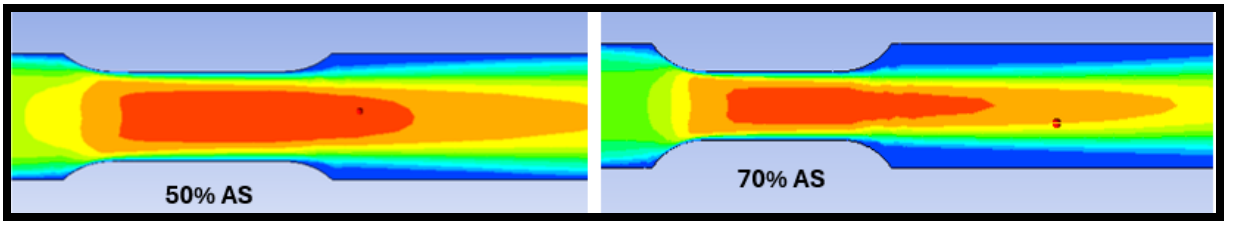


Figure 27: Zoomed image of velocity contours at first stenotic throat: Newtonian Flow

This jet formation can be clearly seen at the throats for both cases, with the 50% AS jet appearing shorter and broader, while the 70% AS jet is more elongated and narrower. In 50% AS case, the high velocity core, shown by red and orange colour, is spread out gently as it moves downstream, blending into yellow and then green. On the other hand, the 70% AS jet is much narrower and more intense, with a strong red core that extends further downstream and is sharply bordered by orange and yellow. This suggests that as stenosis severity increases, the jet becomes more focused and intensified, leading to more energetic and possibly turbulent flow after the stenosis. The two models exhibit milder acceleration, with flow remaining more stable post-stenosis. In contrast, the 90% AS shows some distinctions when comparing the first stenosis, the flow at the throat is extremely concentrated and high-speed, but rather than a typical jet that gradually dissipates, this one remains highly confined and extends much further downstream. Red and orange regions seem to be tightly packed, which may indicate a high momentum core that dominates the flow. With this extreme narrowing, however, the flow immediately downstream is more prone to instabilities, recirculation, and turbulence. During the systolic phase, the velocity reaches its maximum at 2.03 m/s, which is almost four times greater than the velocity at the inlet. This increase highlights the impact of severe stenosis on flow dynamics within the artery. Comparing the Newtonian and Non-Newtonian (Carreau) models, for all three stenotic severity cases, the results show minimal differences in peak velocities. However, the Carreau model, which accounts for the shear-thinning behaviour of blood, consistently predicts slightly lower velocities, indicating a smoother velocity transition between high and low flow regions. This could be due to the mathematical model's ability to capture the viscosity variations of blood, where at low shear rates, blood behaves as a more viscous fluid, and at high shear rates, its viscosity decreases. This dynamic response prevents the excessive acceleration of flow, leading to a more physiologically accurate representation of blood flow behaviour. Conversely, the Newtonian model, which assumes constant viscosity, was observed to nominally overestimate the velocity in the stenotic region, resulting in sharper gradients. These findings align with those of Guerciotti & Vergara [29], where small differences between Newtonian and non-Newtonian models were noted when comparing systolic velocities. Figure 28 shows the relationship between maximum velocity magnitude and the power-law index (n) for the Carreau model. An increasing trend is observed, as the power-law index (n) increases, the maximum velocity also increases for all three stenotic levels. Notably, higher area stenosis percentages lead to significantly greater velocities, with the 90% AS case exhibiting the highest values, followed by 70% AS and 50% AS.

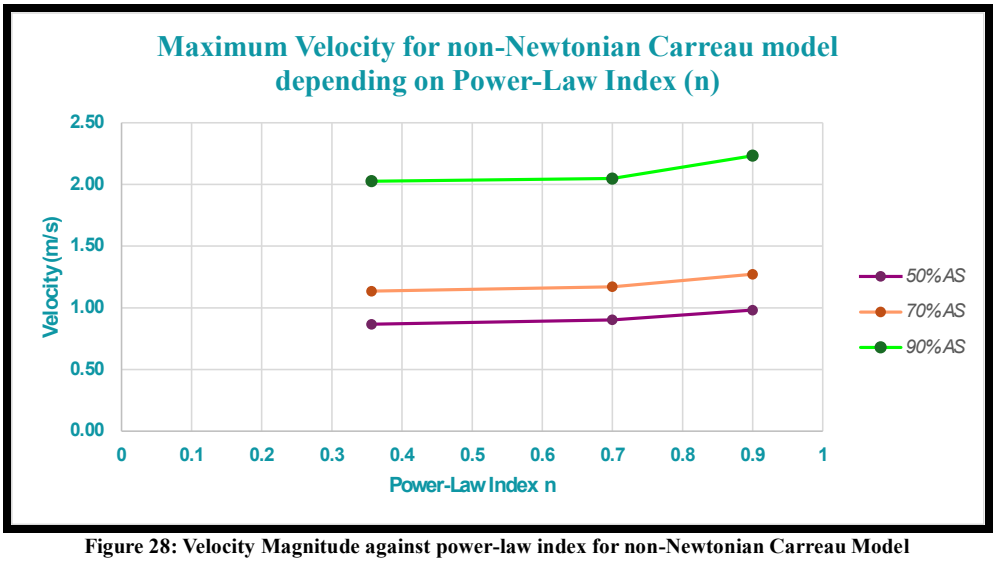


Figure 28: Velocity Magnitude against power-law index for non-Newtonian Carreau Model

The velocity differences become more pronounced as n increases, suggesting that the blood shear-thinning behaviour plays an important role in velocity distribution. As the severity of stenosis increases, the results indicate a

significant rise in velocity, which may elevate the risk of the onset of chaotic, turbulent flow and lead to adverse hemodynamic effects.

4.2. Pressure Contours

Figures 29-46 display the contours of pressure in the dual stenotic arterial regime. Again, we consider intermediate (50%) i.e. Figs 29-34, strong (70%) i.e. Figs. 35-40 and chronic stenosis (90%) i.e. Figs 41-46, in turn. As with the velocity contours described earlier, each stenosis severity case has 6 plots - *Newtonian, non-Newtonian, Newtonian Systolic, Newtonian Diastolic, non-Newtonian Systolic and non-Newtonian Diastolic.* The pressure contours indicate a pressure drop at the stenosis region for all cases, which becomes more severe with increasing stenosis depth. This drop is a direct result of flow acceleration at the stenosis. As the cross-sectional area decreases within the stenosis, the fluid (blood) must accelerate to maintain a constant flow rate. This acceleration requires a conversion of pressure energy into kinetic energy, leading to a reduced static pressure at the constriction. This phenomenon is also referred to as the Venturi effect, where a narrowing of the flow passage (stenosis) causes an increase in flow velocity and a corresponding decrease in pressure. The more severe the narrowing, the greater the velocity increase and pressure drop. This was also shown by Kamangar et al. [5], where the authors concluded a higher degree of pressure drop at 90% AS compared to 70% AS.

4.2.1. 50% Area Stenosis (AS)

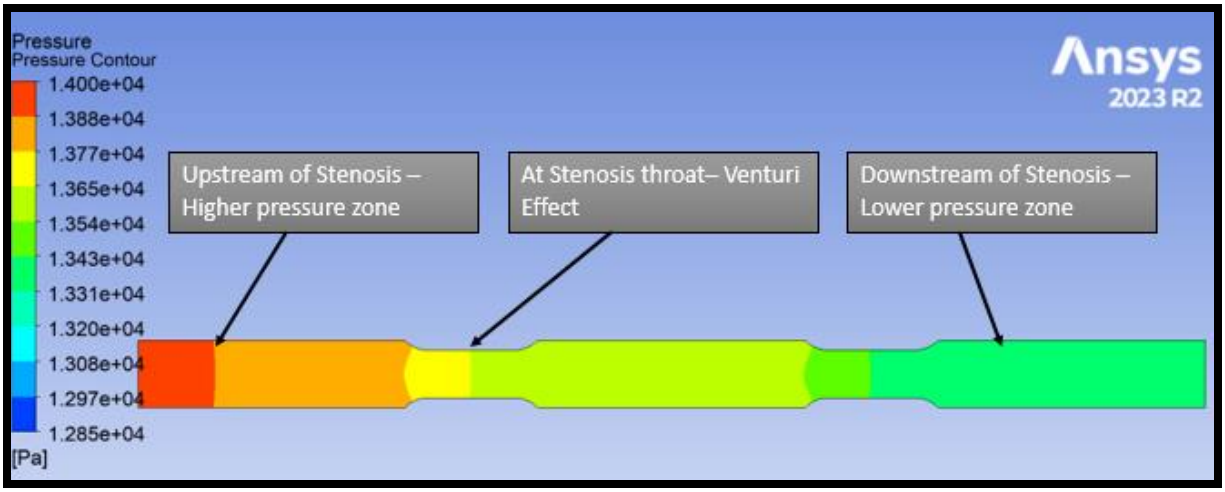


Figure 29: Pressure at 50% AS: Newtonian Model

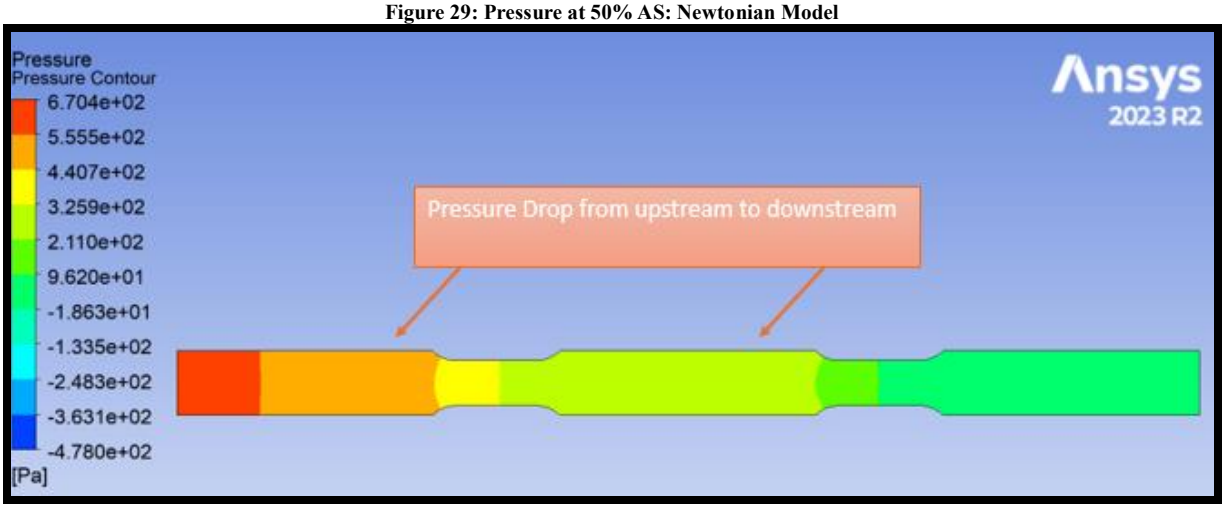


Figure 30: Pressure at 50% AS: non-Newtonian Carreau Model

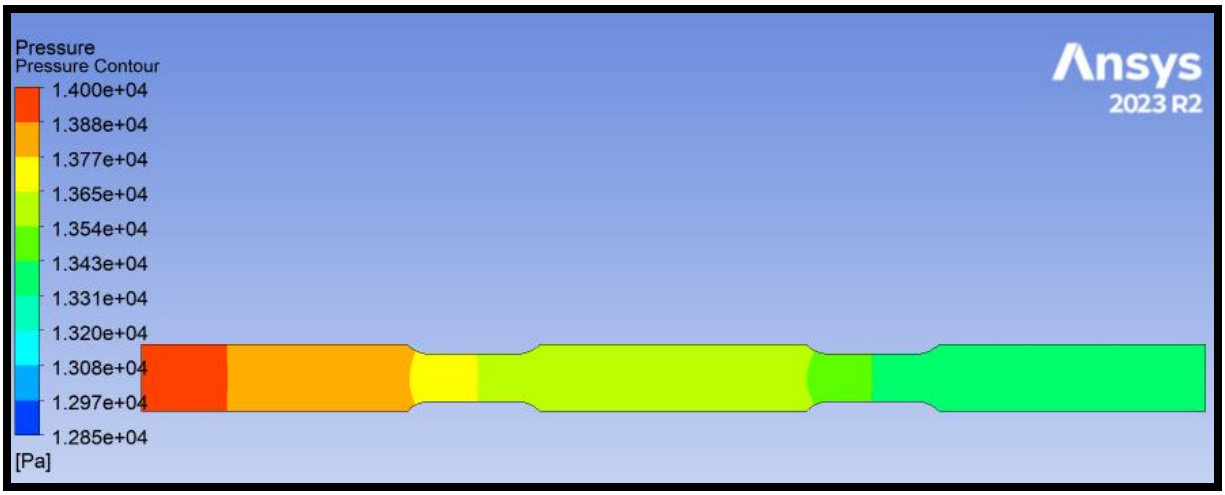


Figure 31: Pressure at 50% AS: Newtonian Systolic

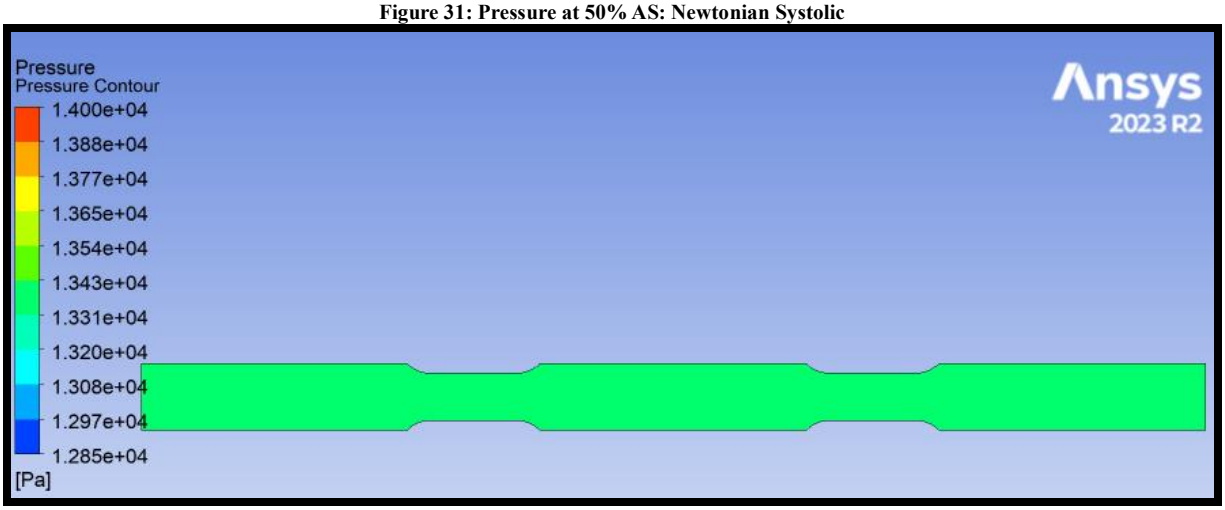


Figure 32: Pressure at 50% AS: Newtonian Diastolic

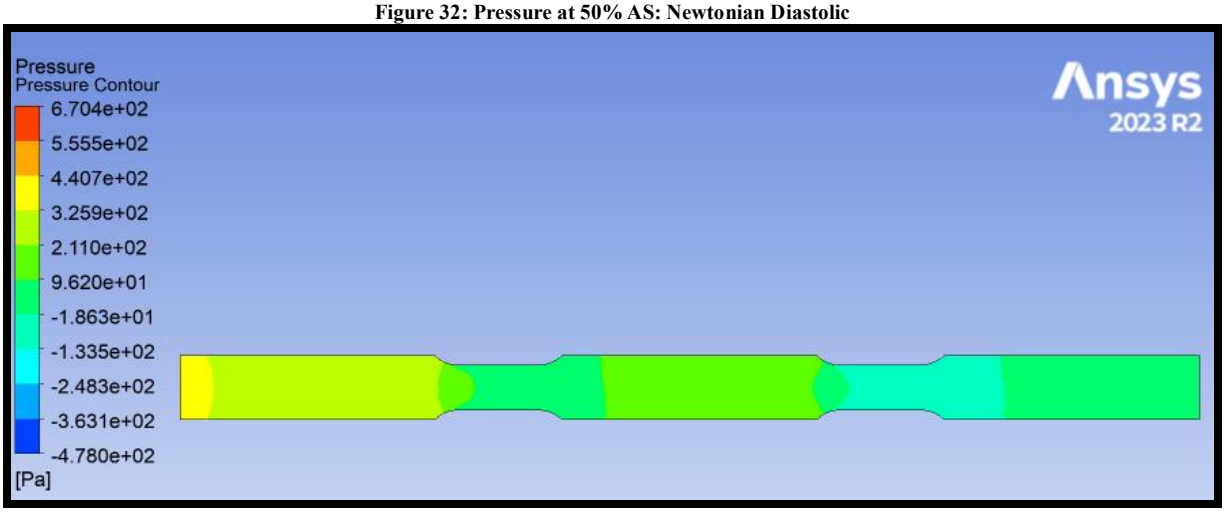


Figure 33: Pressure at 50% AS: non-Newtonian Carreau Systolic

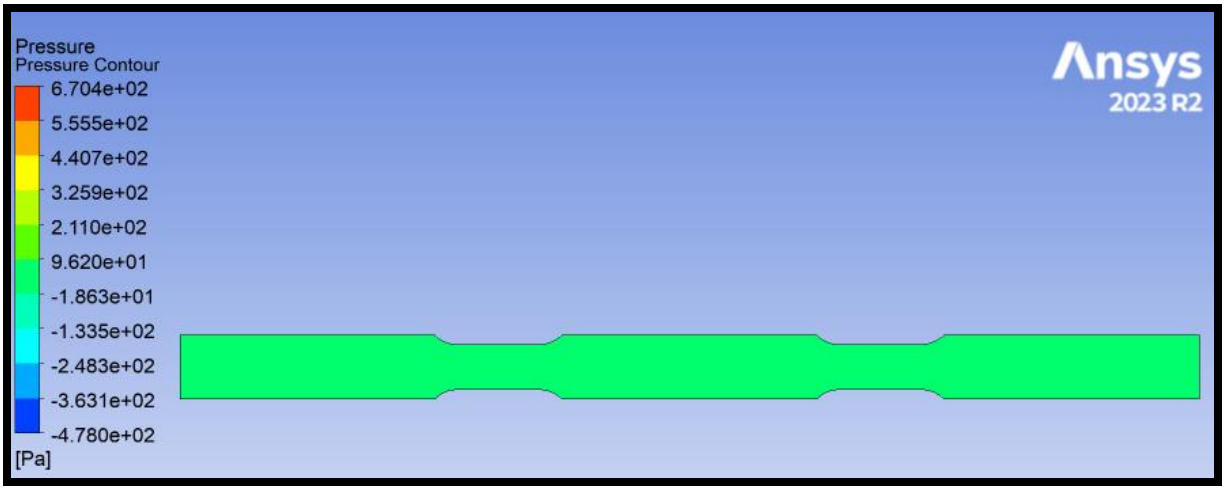


Figure 34: Pressure at 50% AS: non-Newtonian Carreau Diastolic

4.2.2. 70% Area Stenosis (AS)

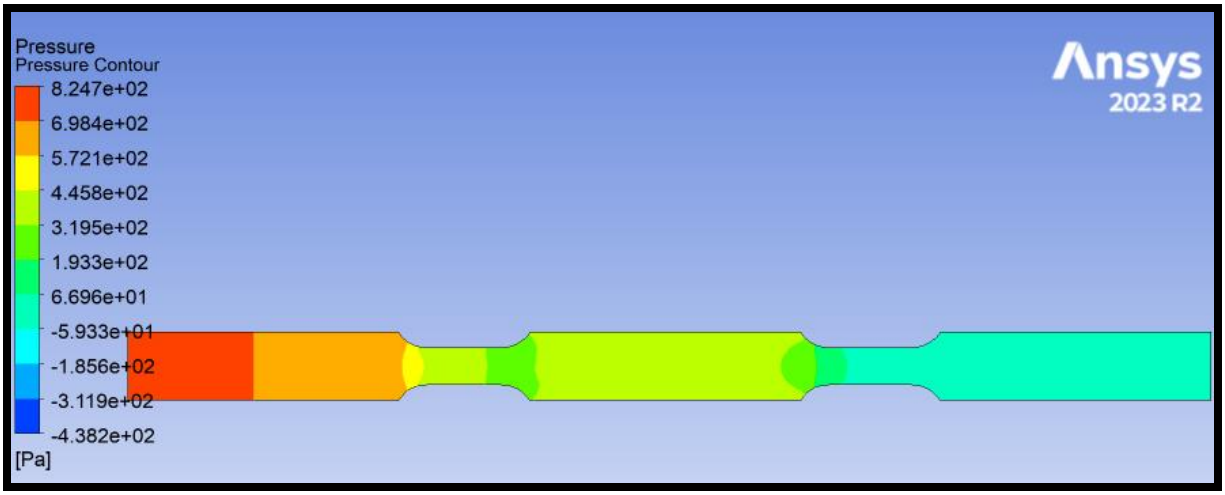


Figure 35: Pressure at 70% AS: Newtonian Model

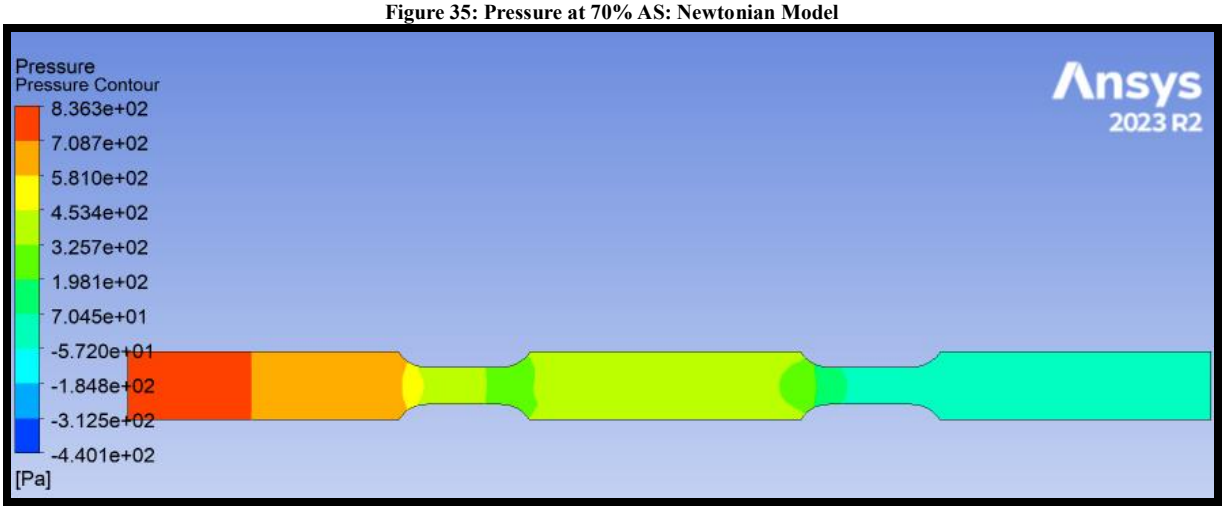


Figure 36: Pressure at 70% AS: non-Newtonian Carreau Model

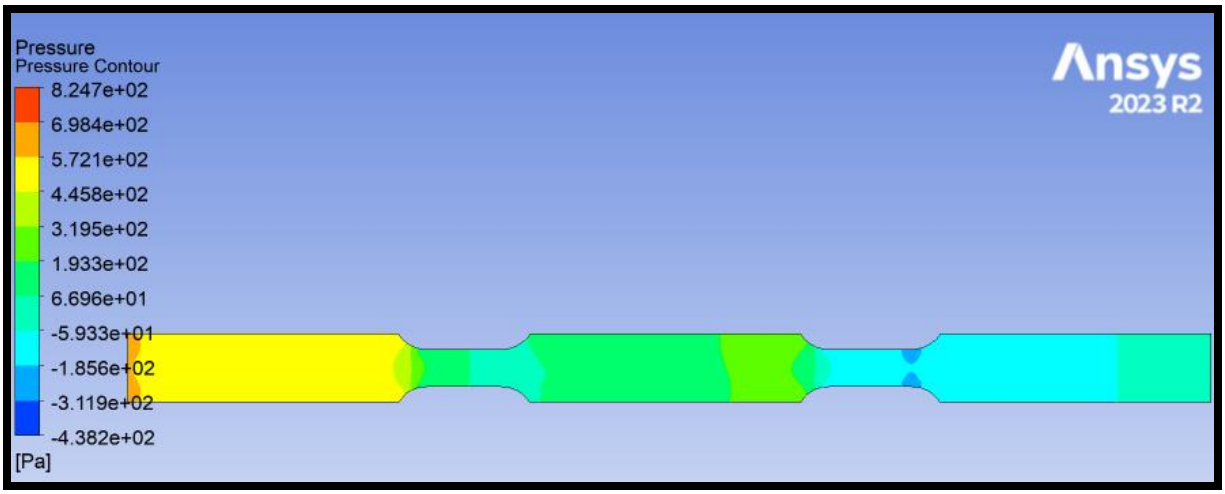


Figure 37: Pressure at 70% AS: Newtonian Systolic

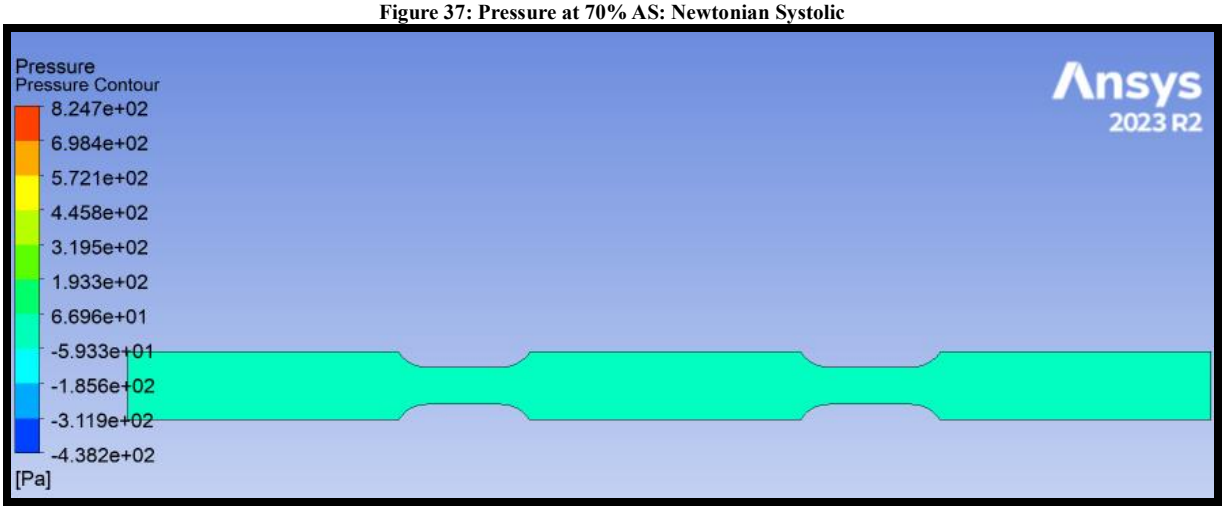


Figure 38: Pressure at 70% AS: Newtonian Diastolic

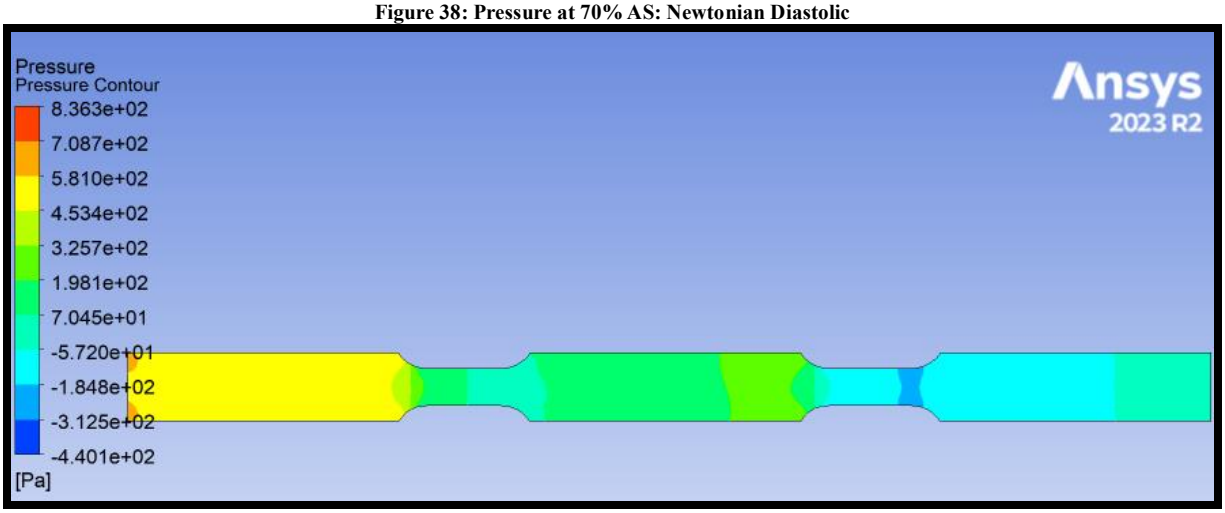


Figure 39: Pressure at 70% AS: non-Newtonian Carreau Systolic

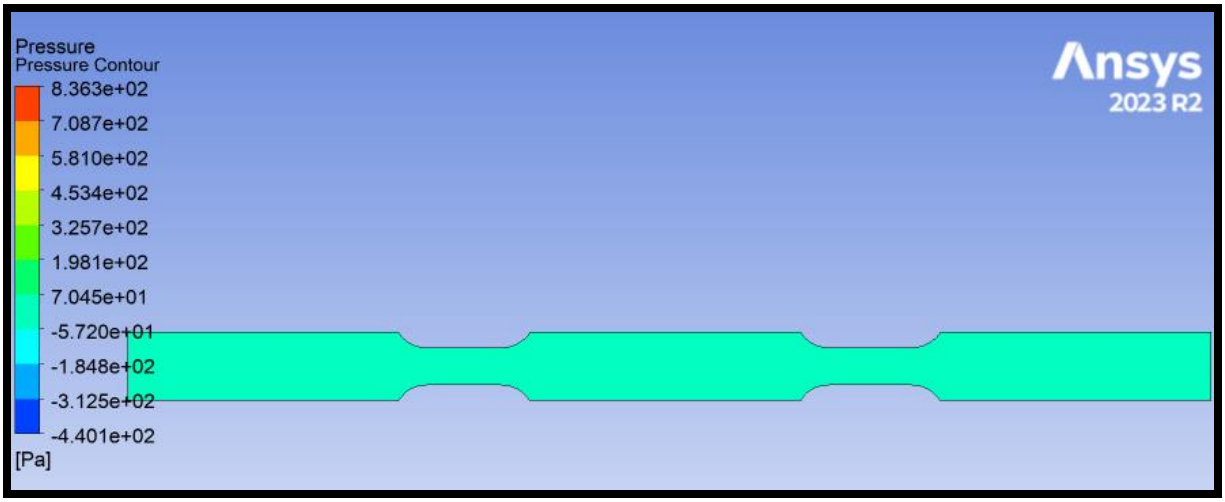


Figure 40: Pressure at 70% AS: non-Newtonian Carreau Diastolic.

4.2.3. 90% Area Stenosis (AS)

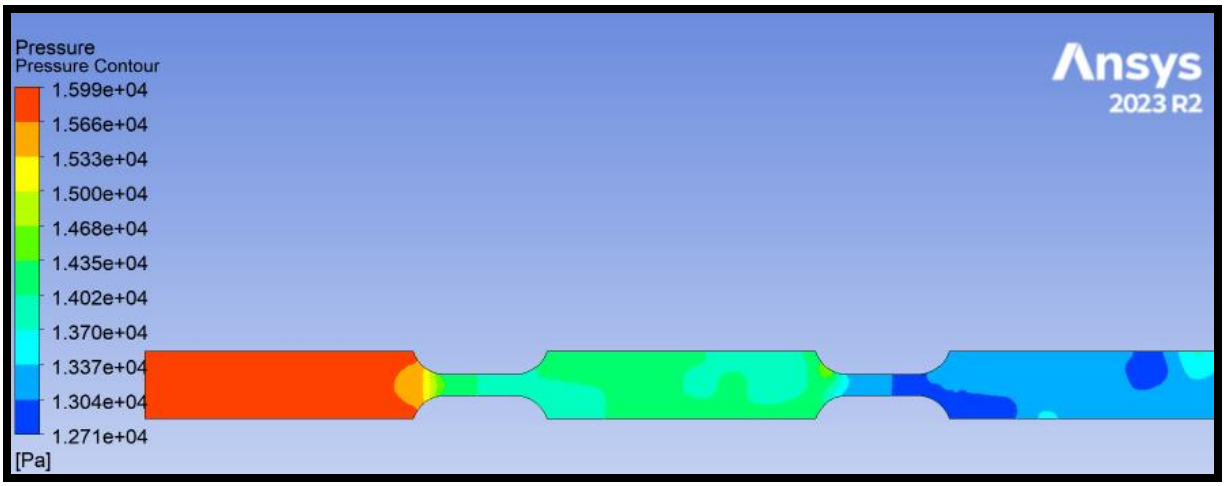


Figure 41: Pressure at 90% AS: Newtonian Model

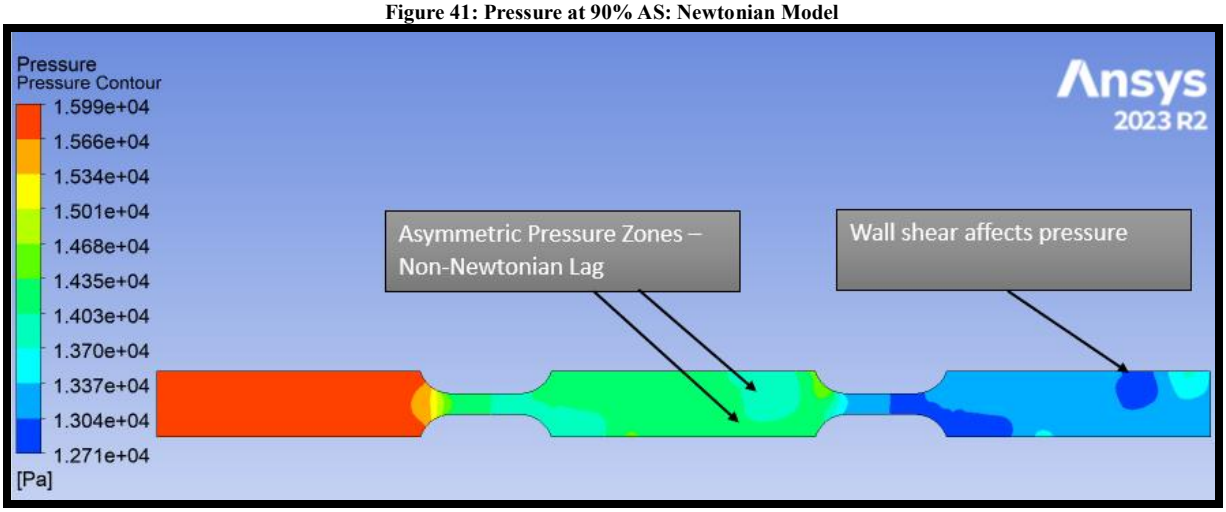


Figure 42: Pressure at 90% AS: non-Newtonian Carreau Model

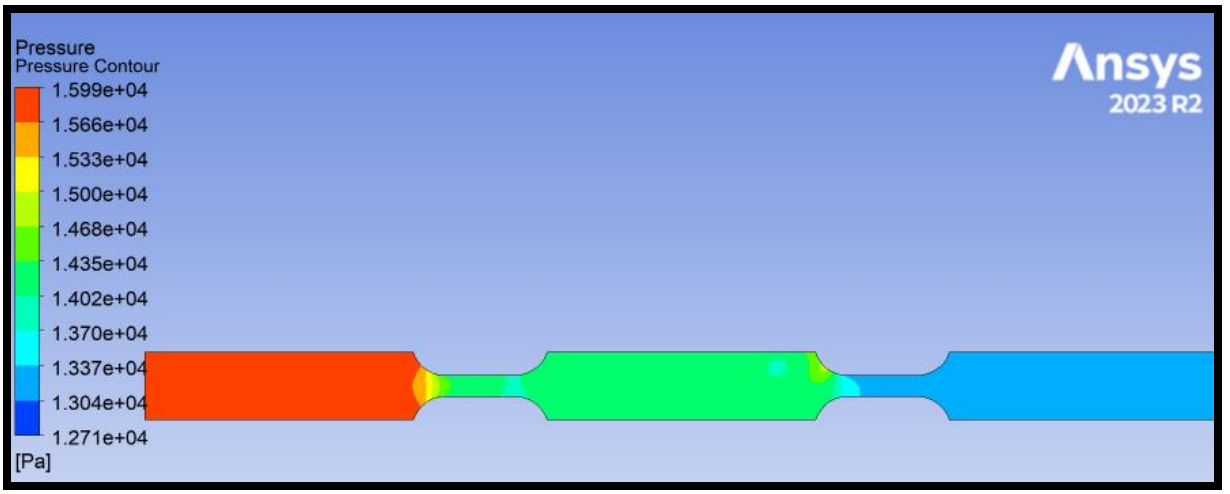


Figure 43: Pressure at 90% AS: Newtonian Systolic

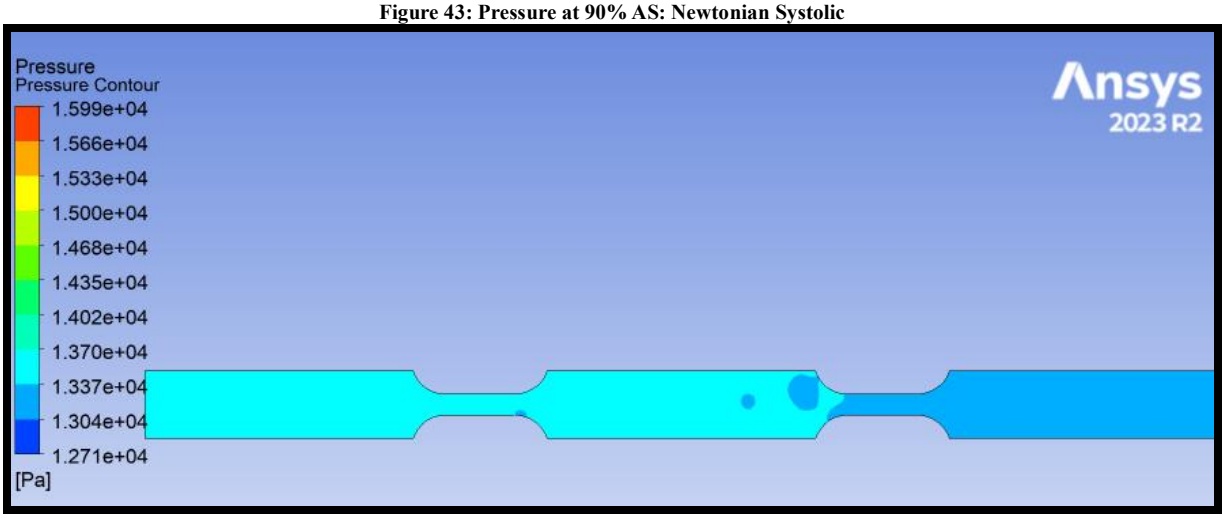


Figure 44: Pressure at 90% AS: Newtonian Diastolic

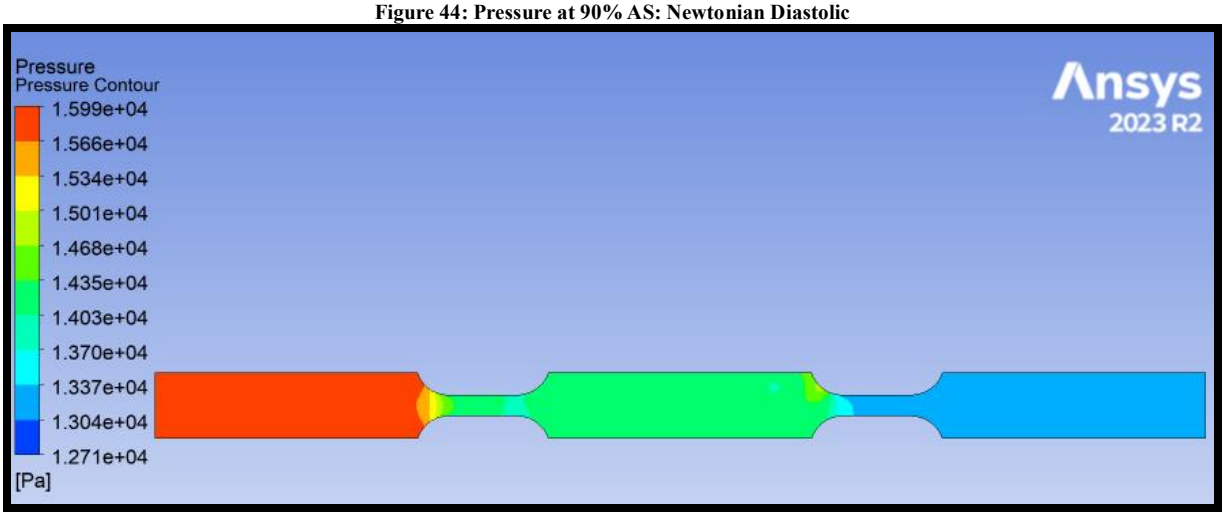


Figure 45: Pressure at 90% AS: non-Newtonian Carreau Systolic

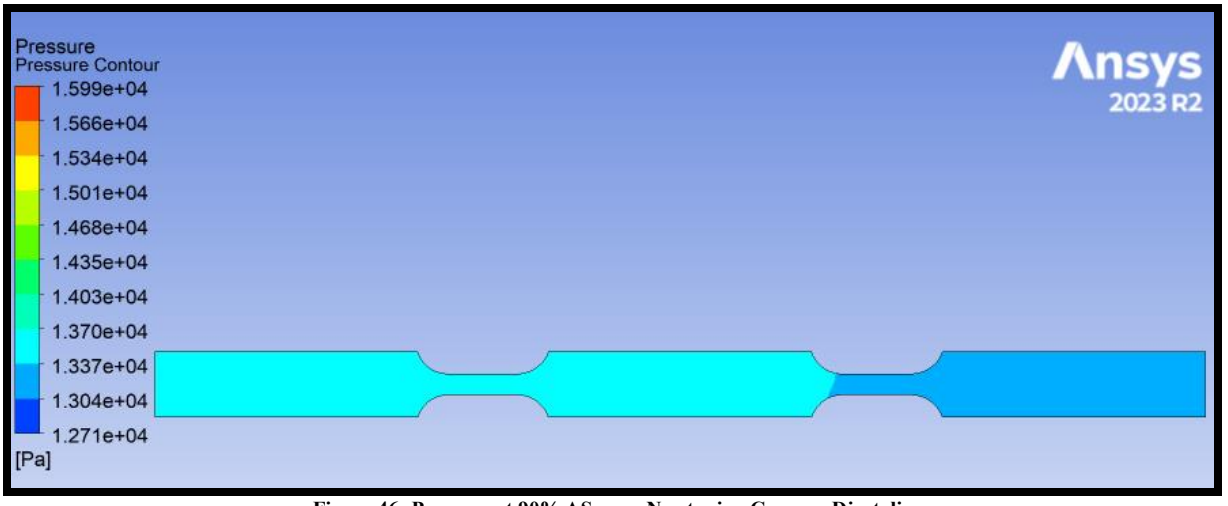


Figure 46: Pressure at 90% AS: non-Newtonian Carreau Diastolic

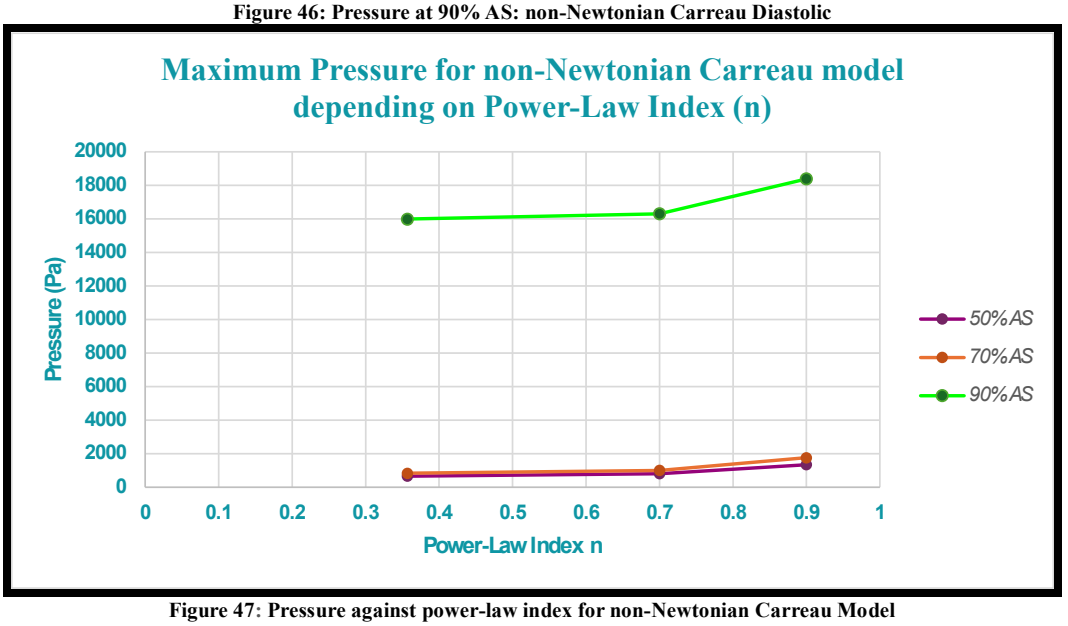


Figure 47: Pressure against power-law index for non-Newtonian Carreau Model

At 90% AS, the pressure drop is significantly higher than at 50% AS because the flow acceleration is higher than at the severe constriction. Within this model, the pressure drop is noted to be considerably higher at the first throat compared to the second throat. This is because the first throat experiences the most flow contraction, causing a larger pressure gradient. As the fluid moves past the first throat and enters the second constriction, some energy is already dissipated due to turbulence and viscous effects, leading to a relatively lower pressure drop at the second throat. These findings also align well with the study by Kabir et al. [30] who found that the pressure values remain higher at the first throat for all stenosis levels compared to the second throat. Additionally, flow separation and recirculation zones downstream of the stenosis may contribute to further energy losses. These become more prominent at higher degrees of stenosis, where disturbed flow patterns and vortex formation increase resistance, increasing the pressure drop. Interestingly, the post-stenotic pressure recovery is more explicit in moderate stenosis cases but remains minimal in the 90% AS model, with asymmetrical regions more prominent, suggesting higher flow disturbance. Figure 47 depicts the relationship between maximum pressure and the Power-Law Index (n) for the Carreau model, showing a trend similar to that observed for velocity magnitude against n. The maximum pressure rises as n increases for all stenosis levels. 90% AS (green curve) shows significantly higher pressure compared to 50% and 70% AS. Between the 50% curve (purple) and the 70% curve (orange), the pressure difference remains relatively small. A sharp increase is also notable for n = 0.9, particularly for 90% AS This could be attributed to blood's rheological behaviour at a higher power-law index. In a non-Newtonian mathematical equation for the Carreau model (4), a higher n means the fluid exhibits less shear-thinning behaviour, approaching Newtonian characteristics. Hence, the viscosity remains relatively higher under shear stress, leading to an increased resistance to flow and, in return, an increased pressure buildup.

4.3. Wall Shear Stress (WSS)

Since the CFD simulations were carried out on 2D models/geometries, contour plots were unavailable. However, the maximum values for 50%, 70% and 90% area stenosis were extracted and compared in a bar chart (**Figure 48**). The results show that generally, WSS increases with higher stenosis, with both fluid models exhibiting nearly identical values across all stenosis levels. This may suggest that shear-thinning effects in the non-Newtonian model do not significantly alter WSS compared to the Newtonian case. A likely explanation could be that at the region of maximum WSS, which is typically at the stenosis throat as noted by Kabir et al. [30], the shear rates are already high enough for the non-Newtonian Carreau fluid to behave similarly to a Newtonian fluid, as its viscosity approaches a nearly constant asymptotic value. At 90% AS, WSS rises sharply, reaching 100 Pa, which is a 150% increase compared to 50% AS. Hence, from this study, it can be concluded that the WSS increases with the severity of constriction within an artery model. This is consistent with many previous studies, like Wu et al. [7] and Dubey et al. [12]. Wall shear stress plays a crucial role in endothelial damage and plaque rupture risk. Clinical studies, such as those by Malek et al. [31], have shown that elevated WSS can contribute to endothelial dysfunction and atherosclerosis progression. It is crucial to understand WSS particularly its role in arteries, studies suggest that regions of extremely high WSS, such as those found in severe arterial stenosis (e.g., 90% AS), may weaken plaques by inducing structural changes in the fibrous cap, making them more prone to rupture as elaborated by Eshtehardi et al. [32]. This is extremely concerning since plaque rupture is a primary cause of acute coronary syndromes, leading to blood clots and thrombosis, as highlighted by Loftus [33]. Conversely, low WSS has been associated with plaque development due to recirculation and stagnation of flow. Therefore, understanding the relationship between wall shear stress (WSS) and plaque is essential for improving predictive models of cardiovascular diseases and the development of interventions, such as stents and pharmaceutical therapies.

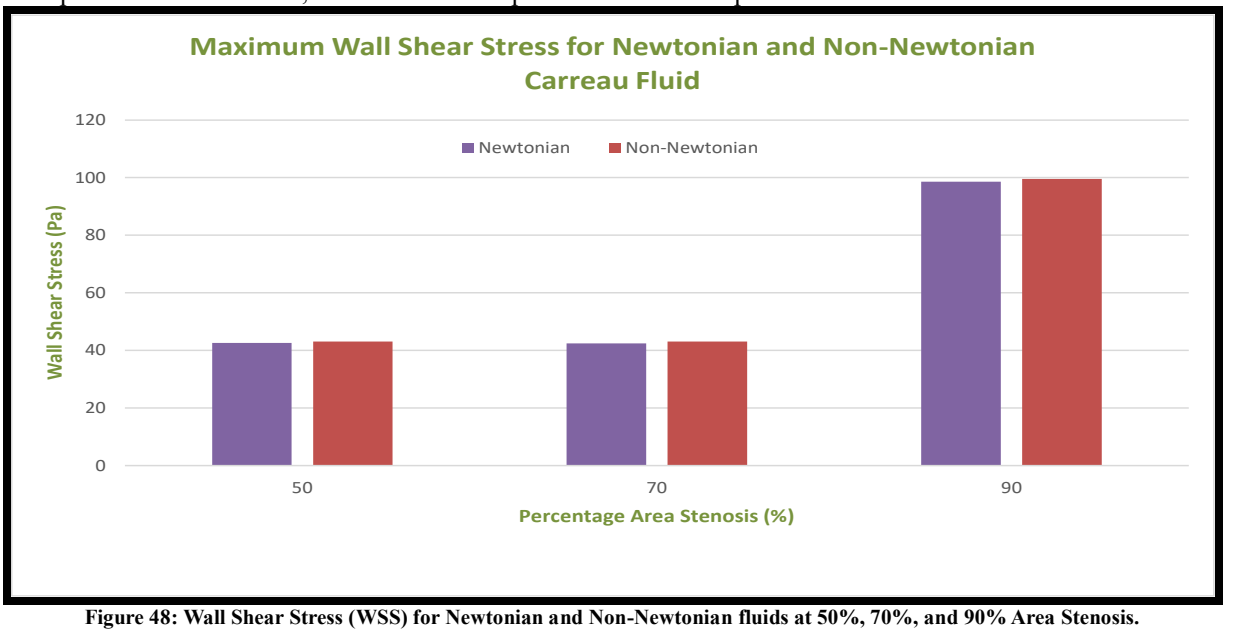


Figure 48: Wall Shear Stress (WSS) for Newtonian and Non-Newtonian fluids at 50%, 70%, and 90% Area Stenosis.

4.4. Vorticity Contours

Vorticity magnitude contour plots (**Figures 49-54**) highlight key flow characteristics in the artery models. Here we consider intermediate (50%) i.e. **Figs 49-50**, strong (70%) i.e. **Figs. 51-52** and chronic stenosis (90%) i.e. **Figs 52-53**, in turn. However, *only 2 plots – Newtonian and non-Newtonian are included for each stenotic severity case.* Pre-stenosis, a low-intensity vorticity zone is observed, suggesting relatively stable and uniform flow before the constriction. However, as the fluid approaches the stenotic throat, vorticity increases sharply, reaching its maximum value along the throat wall (as shown by the red and orange colours in the contours). This high vorticity at the throat is caused by the abrupt narrowing, which induces strong shear forces.

4.4.1. 50% Area Stenosis (AS)

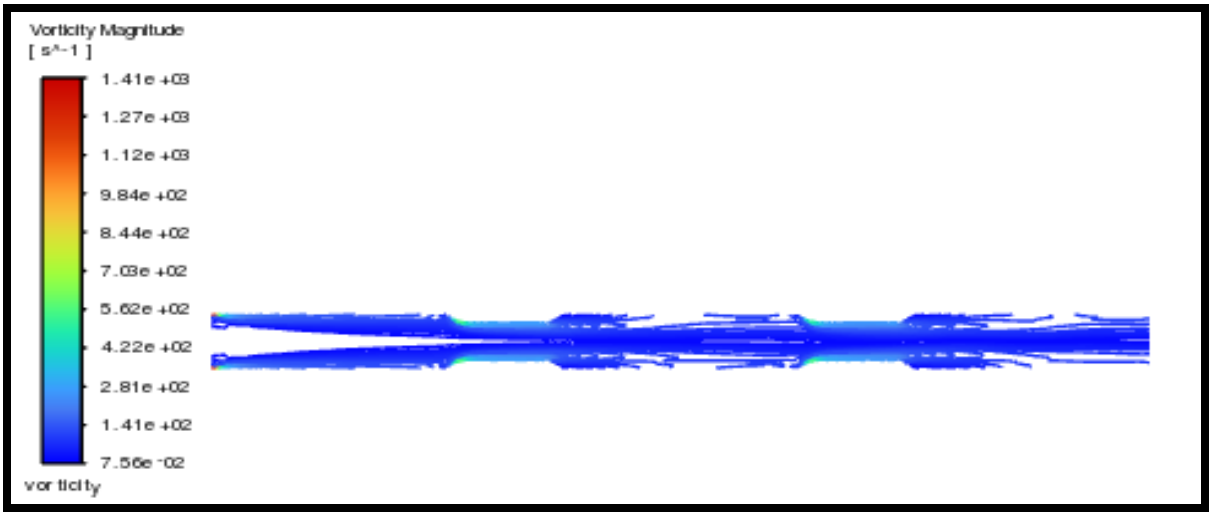


Figure 49: Vorticity Magnitude at 50% AS: Newtonian Model

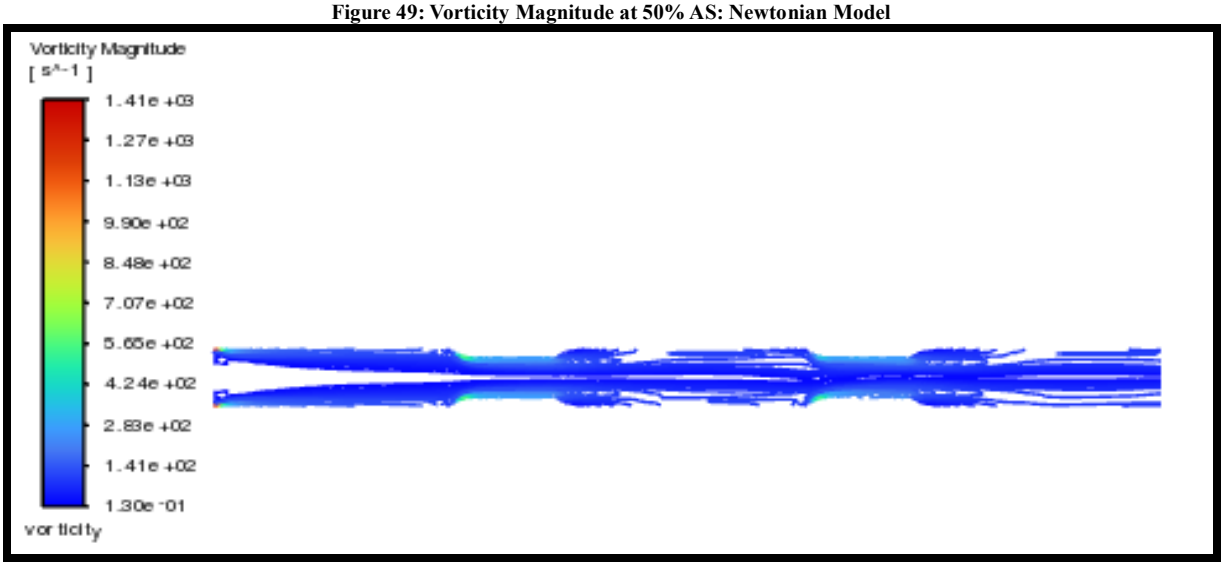


Figure 50: Vorticity Magnitude at 50% AS: non-Newtonian Carreau Model

4.4.2. 70% Area Stenosis (AS)

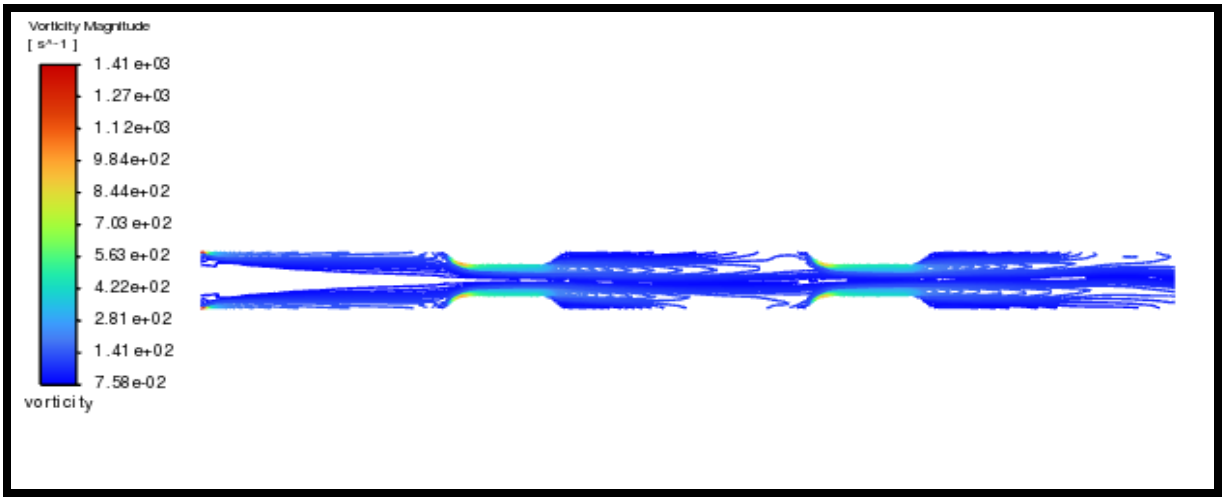


Figure 51: Vorticity Magnitude at 70% AS: Newtonian Model

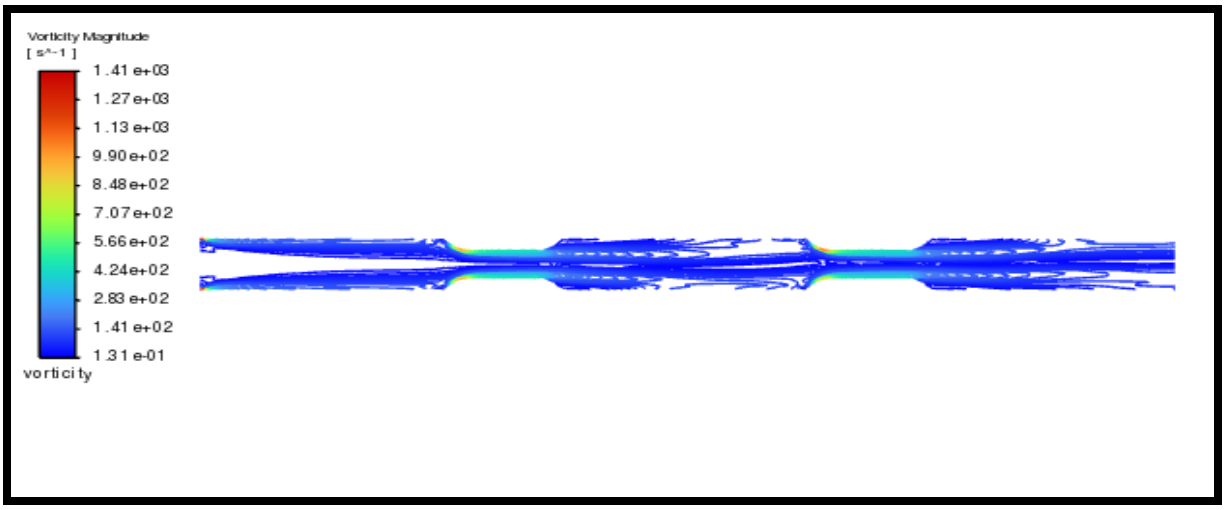


Figure 52: Vorticity Magnitude at 70% AS: non-Newtonian Carreau Model

4.4.3. 90% Area Stenosis (AS)

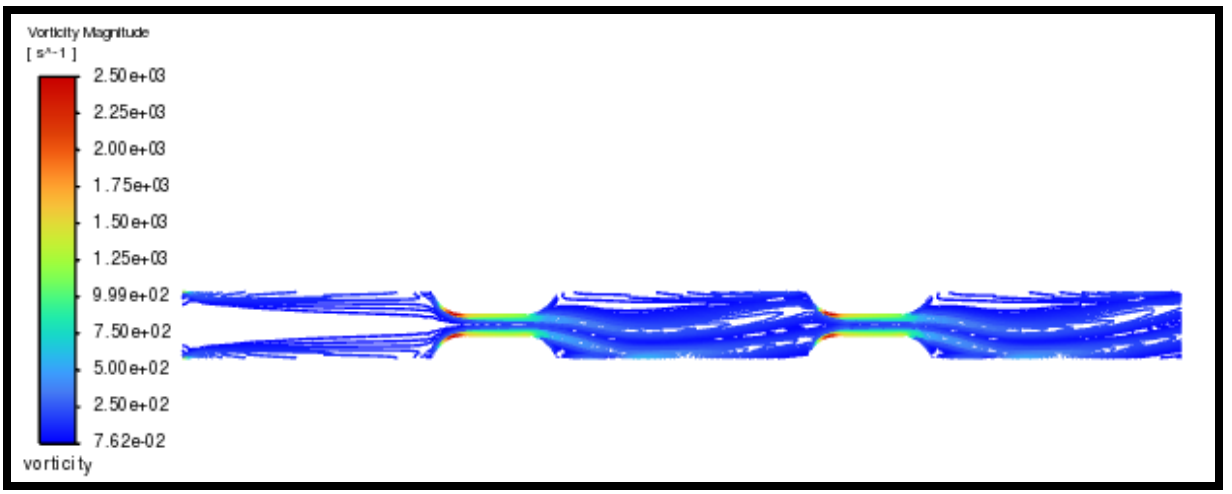


Figure 53: Vorticity Magnitude at 90% AS: Newtonian Model

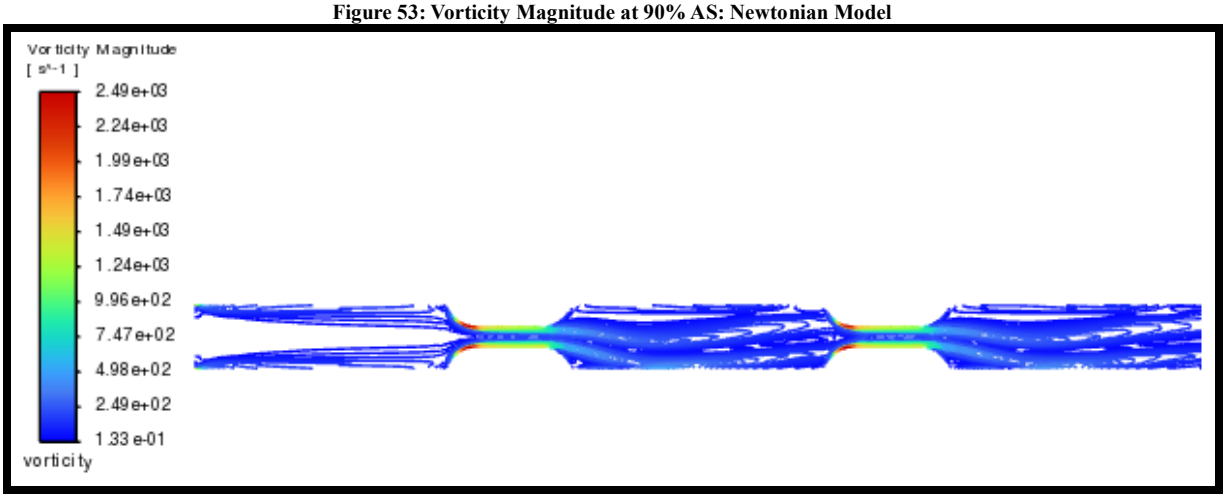


Figure 54: Vorticity Magnitude at 90% AS: non-Newtonian Carreau Model

Additionally Figure 55 provides a zoom shot of the vorticity magnitude plot of 90% AS for the *Newtonian case* at the *first stenosis*, where flow separation can be observed immediately post-stenosis, leading to recirculation zones.

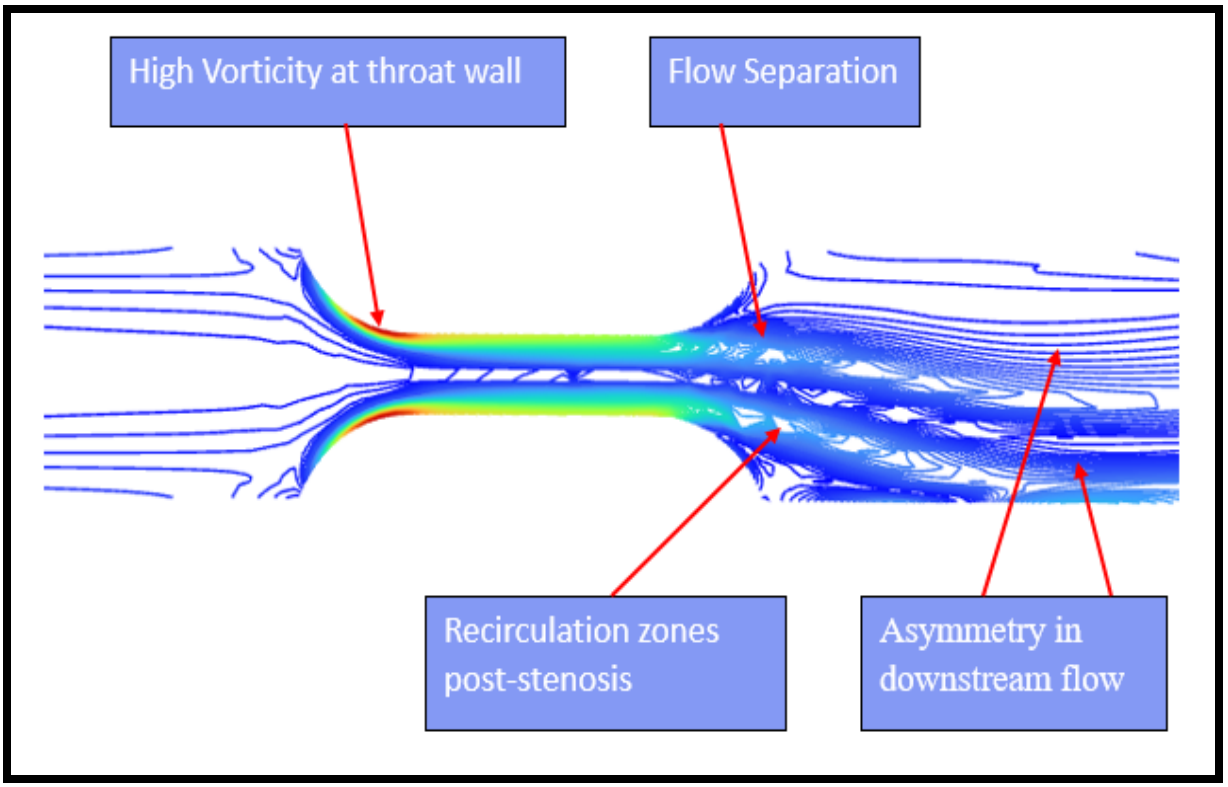


Figure 55: Vorticity Magnitude at 90% AS: Newtonian Model (zoomed at first stenosis)

The streamlines can be seen breaking away from the jet; here, the local flow reverses and forms eddies or vortical structures. These vortices can contribute to flow instability and increase the risk of thrombus formation as described by Naim et al. [34]. We note that vorticity (ω) in a fluid flow is defined as the curl of the velocity vector field and is mathematically expressed as $\omega = \nabla \times v$ where ω is the vorticity at a point in the blood flow, ∇ is the Laplacian operator, and v is the velocity vector at a given point. The stenosis is a region of high shear, where vorticity tends to increase significantly due to abrupt changes in flow velocity. As the fluid enters the constricted section, the velocity increases rapidly as it is forced through the narrow passage. This sharp change in velocity leads to the formation of strong velocity gradients across the flow, resulting in high shear stress at the walls of the artery. This change in velocity causes the fluid particles to rotate and swirl, creating vortical structures that contribute highly to flow instability. As observed in Figure 55, flow separation and recirculation zones form immediately post-stenosis, suggesting high vorticity regions. Additionally, in the highly disturbed flow regions downstream of the stenosis, the flow becomes increasingly asymmetric, likely due to uneven velocity distribution and turbulence effects. As the high-velocity jet exits the stenotic region, it interacts with the slower-moving surrounding fluid, creating a shear layer that destabilises the flow. This results in an uneven velocity distribution, where one side of the vessel may experience higher velocities while the other is dominated by low-momentum recirculating flow. A negligible difference in vortex magnitude is however observed between Newtonian and non-Newtonian fluids and this is corroborated by other studies including Guerciotti and Vergara [29].

5. CONCLUSIONS AND FUTURE PATHWAYS

This article has examined computationally the laminar hemodynamic behaviour of blood in 2-dimensional multi-stenotic arteries using both Newtonian and non-Newtonian (Carreau) models in ANSYS Fluent. The geometric models have featured two stenotic regions. The Carreau model was selected for its accuracy in simulating shear-thinning fluids to capture the dynamic nature of blood flow. The main findings of these 2-D simulations can be summarized below:

(i). Across all stenosis levels (50%, 70%, and 90%), flow velocity peaked within the throat region due to the narrowing of the artery. A jet formation was observed for 50% and 70% models while 90% model showed the maximum velocity at the stenotic.

(ii). The Newtonian model slightly overestimated peak velocities and showed steeper gradients compared to the Carreau model, which demonstrated smoother velocity transitions due to its variable viscosity.

(iii). Pressure dropped significantly at the stenotic throats, especially at the first narrowing in each geometry. This expected pressure drop was due to the Venturi effect and increased with the severity of stenosis.

(iv). The Carreau model indicated higher pressure gradients at higher power-law indices *n*, which possibly corresponded to reduced shear-thinning behaviour.

(v). Wall shear stress (WSS) was found to increase substantially with higher degrees of stenosis. The maximum WSS reached 100 Pa at 90% stenosis, underlining the known link between elevated WSS and increased risk of endothelial damage and plaque rupture.

(vi). A severe stenosis induced strong vortical structures downstream of the constriction, especially in the 90% model. These regions of recirculating flow and flow separation were associated with asymmetry and instability in the post-stenotic regions.

(vii). Differences between Newtonian and non-Newtonian models were minimal for WSS and vorticity at high shear rates, suggesting that under such conditions, the shear-thinning behaviour of blood becomes less pronounced, and its viscosity approaches the Newtonian approximation.

The present simulations have revealed some complex intricate flow structures in multi-stenosed arterial non-Newtonian and Newtonian blood flows. However certain approximations have been made. The arterial walls were assumed to be rigid, whereas the natural blood vessels are elastic, they expand and contract with pulsatile blood flow. This flexibility will influence velocity profiles, pressure distributions, and wall shear stress, potentially altering the predictions made in the simulations. Since arterial walls are compliant and deform under pulsatile pressure, FSI allows for a two-way coupling between the fluid flow and the arterial wall, which leads to more realistic simulations of stress distribution and arterial response. A good example of this integration would be the study by (Kuharat *et al.* [19]), where CFD and FSI were deployed to investigate the plaque buildup in stenotic arteries. Also, the current study has assumed arterial models to be *straight and uniform*, whereas actual arteries, particularly in regions prone to stenosis (e.g., carotid and coronary arteries), are often curved or bifurcated. Curvature introduces secondary flows, such as Dean vortices, which can significantly influence flow separation and turbulence in stenosed vessels (Bég et al. [35]). More complex arterial geometries, such as curved or helical stenotic arteries, may be considered in future studies. Unlike straight arteries, these configurations can introduce secondary flow patterns and centrifugal forces that can significantly alter hemodynamic behaviour, as elaborated by Hong et al. [36]. Additionally, the present study used a very generic arterial model, which means the findings may be broadly applicable, but may not capture specific arterial hemodynamic. Individual factors such as vessel diameter, length, shape or plaque composition significantly alter and influence blood flow behaviour. In clinical studies, patient-specific models reconstructed from MRI or CT scans would highly increase the dependency of simulated results and make them more useful for personalised treatment. There is future scope also to investigate tapered, diverging or converging arterial geometries, which more closely reflect diseased arteries that change shape progressively rather than abruptly. The present ANSYS FLUENT simulations have also neglected the transport of oxygen and other nutrients in the blood. As a result, the effect of altered flow patterns on oxygen delivery and potential ischemic regions (areas of tissue with a lack of oxygen and nutrients, leading to reduced blood flow) cannot be evaluated. It is also noteworthy that more complex non-Newtonian models could be explored such as *Eringen's micropolar non-Newtonian model* (as deployed by Vasu et al. [37]), which considers micro-rotation and spin of blood particles and turbulent flow behaviour may also be assessed (in the post-stenotic zone, high-velocity gradients and flow separation can induce transitional or turbulent flow, particularly in larger arteries like carotid bifurcations or coronary arteries). To add further rigour to simulations, experimental validation techniques such as time-resolved Particle Image Velocimetry (PIV) could also be utilized in future studies. This technique can provide high-resolution flow data, capturing transient velocity fields in physical arterial models, that can be compared with CFD predictions, as elucidated by Tomaszewski et al. [38]. All these potential pathways could be investigated in future studies and are currently under consideration.

References

[1] H. R. Institute. *Heart Research Institute*, Accessed 19 October 2026; https://www.hriuk.org/.

[2] P. Geoghegan, N. Buchmann, J. Soria, M. C. Jermy, Time-resolved PIV measurements of the flow field in a stenosed, compliant arterial model, *Experiments in fluids,* Vol. 54, No. 5, pp. 1528, 2013.

[3] J. Banks, N. Bressloff, Turbulence modeling in three-dimensional stenosed arterial bifurcations, 2007.

[4] A. Aghaee, M. O. Khan, Pinning down the accuracy of physics-informed neural networks under laminar and turbulent-like aortic blood flow conditions, *Computers in Biology and Medicine,* Vol. 185, pp. 109528, 2025.

[5] S. Kamangar, N. Ameer Ahamad, N. Nik-Ghazali, A. E. Anqi, A. Algahtani, C. Ahamed Saleel, S. Javed, V. Tirth, T. Yunus Khan, The influence of multi-stenosis in the left coronary artery subjected to the variable blood flow rate, *Frontiers in Engineering and Built Environment,* Vol. 1, No. 1, pp. 97–106, 2021.

[6] S. Akhtar, Z. Hussain, S. Nadeem, I. R. Najjar, A. Sadoun, CFD analysis on blood flow inside a symmetric stenosed artery: Physiology of a coronary artery disease, *Science progress,* Vol. 106, No. 2, pp. 00368504231180092, 2023.

[7] J. Wu, G. Liu, W. Huang, D. N. Ghista, K. K. Wong, Transient blood flow in elastic coronary arteries with varying degrees of stenosis and dilatations: CFD modelling and parametric study, *Computer Methods in Biomechanics and Biomedical Engineering,* Vol. 18, No. 16, pp. 1835–1845, 2015.

[8] J. Yang, Y. Zhang, J. Xue, Y. Guo, S. Liu, Y. Yao, H. Zhong, A. Quan, J. Yang, Hemodynamic effects of stenosis with varying severity in different segments of the carotid artery using computational fluid dynamics, *Scientific Reports,* Vol. 15, No. 1, pp. 4896, 2025.

[9] H. Liu, L. Lan, J. Abrigo, H. L. Ip, Y. Soo, D. Zheng, K. S. Wong, D. Wang, L. Shi, T. W. Leung, Comparison of Newtonian and non-Newtonian fluid models in blood flow simulation in patients with intracranial arterial stenosis, *Frontiers in physiology,* Vol. 12, pp. 718540, 2021.

[10] S. Singh, S. R. Shah, Understanding blood flow in stenosed arteries: Newtonian and non-Newtonian fluid comparisons, *Research Review International Journal of Multidisciplinary,* Vol. 10, No. 1, pp. 203–215, 2025.

[11] J. L. Marpaung, Modeling arterial blood flow under stenosis: a comparative study of Newtonian and Carreau-Yasuda Non-Newtonian approaches, *Journal of Research in Mathematics Trends and Technology,* Vol. 6, No. 2, pp. 88–98, 2024.

[12] A. Dubey, B. Vasu, O. Anwar Bég, R. S. Gorla, A. Kadir, Computational fluid dynamic simulation of two-fluid non-Newtonian nanohemodynamics through a diseased artery with a stenosis and aneurysm, *Computer Methods in Biomechanics and Biomedical Engineering,* Vol. 23, No. 8, pp. 345–371, 2020.

[13] Y. Zhou, C. Lee, J. Wang, The computational fluid dynamics analyses on hemodynamic characteristics in stenosed arterial models, *Journal of Healthcare Engineering,* Vol. 2018, No. 1, pp. 4312415, 2018.

[14] M. Y. Abdollahzadeh Jamalabadi, M. Daqiqshirazi, H. Nasiri, M. R. Safaei, T. K. Nguyen, Modeling and analysis of biomagnetic blood Carreau fluid flow through a stenosis artery with magnetic heat transfer: A transient study, *PLoS One,* Vol. 13, No. 2, pp. e0192138, 2018.

[15] A. G. Rahma, K. Yousef, T. Abdelhamid, Blood flow CFD simulation on a cerebral artery of a stroke patient, *SN Applied Sciences,* Vol. 4, No. 10, pp. 261, 2022.

[16] D. N. Ku, Blood flow in arteries, *Annual review of fluid mechanics,* Vol. 29, No. 1, pp. 399–434, 1997.

[17] A. K. Roy, O. A. Bég, Asymptotic study of unsteady mass transfer through a rigid artery with multiple irregular stenoses, *Applied Mathematics and Computation,* Vol. 410, pp. 126485, 2021.

[18] I. ANSYS, *ANSYS Fluent Theory Guide,* Technical Manual Release 2025 R1 (Version 25.1), ANSYS, Inc., Canonsburg, PA, USA, pp. 2025.

[19] S. Kuharat, M. Chaudhry, O. A. Beg, T. A. Bég, Computational hemodynamic simulation of non-Newtonian fluid-structure interaction in a curved stenotic artery, *European Mechanical Science,* Vol. 8, No. 4, pp. 226–256, 2024.

[20] J. Weisel, R. Litvinov, Red blood cells: the forgotten player in hemostasis and thrombosis, *Journal of Thrombosis and Haemostasis,* Vol. 17, No. 2, pp. 271–282, 2019.

[21] Y. I. Cho, K. R. Kensey, Effects of the non-Newtonian viscosity of blood on flows in a diseased arterial vessel. Part 1: Steady flows, *Biorheology,* Vol. 28, No. 3-4, pp. 241–262, 1991.

[22] G. Shankar, D. Tripathi, P. Deepalakshmi, O. A. Bég, S. Kuharat, E. Siva, A review on blood flow simulation in stenotically diseased arteries, *Critical Reviews™ in Biomedical Engineering,* Vol. 53, No. 5, 2025.

[23] M. E. GENDY, O. A. Bég, A. Kadir, M. Islam, D. Tripathi, Computational fluid dynamics simulation and visualization of Newtonian and non-Newtonian transport in a peristaltic micro-pump, *Journal of Mechanics in Medicine and Biology,* Vol. 21, No. 08, pp. 2150058, 2021.

[24] R. K. Muhammed, H. Basha, G. J. Reddy, U. Shankar, O. A. Bég, Influence of variable thermal conductivity and dissipation on magnetic Carreau fluid flow along a micro-cantilever sensor in a squeezing regime, *Waves in Random and Complex Media,* Vol. 35, No. 7, pp. 13019–13048, 2026.

[25] M. M. Bhatti, O. A. Bég, S. Kuharat, Electromagnetohydrodynamic (EMHD) convective transport of a reactive dissipative carreau fluid with thermal ignition in a non-Darcian vertical duct, *Numerical Heat Transfer, Part A: Applications,* Vol. 86, No. 7, pp. 1896–1926, 2025.

[26] A. Dubey, B. Vasu, O. A. Bég, R. Gorla, Finite element computation of magneto-hemodynamic flow and heat transfer in a bifurcated artery with saccular aneurysm using the Carreau-Yasuda biorheological model, *Microvascular Research,* Vol. 138, pp. 104221, 2021.

[27] L. Goubergrits, K. Affeld, J. Fernandez-Britto, L. Falcon, Geometry of the human common carotid artery. A vessel cast study of 86 specimens, *Pathology-Research and Practice,* Vol. 198, No. 8, pp. 543–551, 2002.

[28] K. J. Beatt, H. E. Luijten, P. J. de Feyter, M. van den Brand, J. H. Reiber, P. W. Serruys, Change in diameter of coronary artery segments adjacent to stenosis after percutaneous transluminal coronary angioplasty: failure of percent diameter stenosis measurement to reflect morphologic changes induced by balloon dilation, *Journal of the American College of Cardiology,* Vol. 12, No. 2, pp. 315–323, 1988.

[29] B. Guerciotti, C. Vergara, *Computational comparison between Newtonian and non-Newtonian blood rheologies in stenotic vessels*, in: *Biomedical Technology: Modeling, Experiments and Simulation*, Eds., pp. 169–183: Springer, 2017.

[30] M. A. Kabir, M. F. Alam, M. A. Uddin, Numerical simulation of pulsatile blood flow: a study with normal artery, and arteries with single and multiple stenosis, *Journal of Engineering and Applied Science,* Vol. 68, No. 1, pp. 24, 2021/11/07, 2021.

[31] A. Malek, Hemodynamic shear stress and its role in atherosclerosis, *JAMA,* Vol. 115, pp. 510–514, 1993.

[32] P. Eshtehardi, A. J. Brown, A. Bhargava, C. Costopoulos, O. Y. Hung, M. T. Corban, H. Hosseini, B. D. Gogas, D. P. Giddens, H. Samady, High wall shear stress and high-risk plaque: an emerging concept, *The international journal of cardiovascular imaging,* Vol. 33, No. 7, pp. 1089–1099, 2017.

[33] I. Loftus, *Mechanisms of Plaque Rupture*, in: R. T. Fitridge, Matthew, *Mechanisms of Vascular Disease: A Reference Book for Vascular Specialists*, Eds., pp. 43–78, Adelaide, Australia: University of Adelaide Press, 2011.

[34] W. N. W. Ab Naim, P. B. Ganesan, Z. Sun, Y. M. Liew, Y. Qian, C.-J. Lee, S. Jansen, S. A. Hashim, E. Lim, Prediction of thrombus formation using vortical structures presentation in Stanford type B aortic dissection: a preliminary study using CFD approach, *Applied Mathematical Modelling,* Vol. 40, No. 4, pp. 3115–3127, 2016.

[35] O. A. Bég, M. M. Hoque, M. Wahiduzzaman, M. M. Alam, M. Ferdows, Spectral numerical simulation of magneto-physiological laminar dean flow, *Journal of Mechanics in Medicine and Biology,* Vol. 14, No. 04, pp. 1450047, 2014.

[36] H. Hong, E. Yeom, H. S. Ji, H. D. Kim, K. C. Kim, Characteristics of pulsatile flows in curved stenosed channels, *PloS one,* Vol. 12, No. 10, pp. e0186300, 2017.

[37] B. Vasu, A. Dubey, O. A. Bég, R. S. R. Gorla, Micropolar pulsatile blood flow conveying nanoparticles in a stenotic tapered artery: Non-Newtonian pharmacodynamic simulation, *Computers in Biology and Medicine,* Vol. 126, pp. 104025, 2020.

[38] M. Tomaszewski, K. Sybilski, P. Baranowski, J. Małachowski, Experimental and numerical flow analysis through arteries with stent using particle image velocimetry and computational fluid dynamics method, *Biocybernetics and Biomedical Engineering,* Vol. 40, No. 2, pp. 740–751, 2020.